STRUCTURAL HEALTH MONITORING FOR SMALL DIAMETER PIPES WITH GUIDED ULTRASONIC WAVE

A Dissertation

by

SHU JIANG

Submitted to the Office of Graduate and Professional Studies of
Texas A&M University
in partial fulfillment of the requirements for the degree of

DOCTOR OF PHILOSOPHY

Chair of Committee,	Sai Lau
Committee Members,	Hong Liang
	Won-Jong Kim
	Hamn-Ching Chen
Head of Department,	Andreas A. Polycarpou

May 2017

Major Subject: Mechanical Engineering

ABSTRACT

The structural health monitoring (SHM) paradigm includes device design for data acquisition and signal processing for defect visualization. An excitation is applied to the interested structure to generate vibration which is measured and analyzed to reveal structural defects. Guided ultrasonic wave (GUW) has proved to be effective as an excitation for shell SHM. Device settings and corresponding signal processing methods have been proposed to detect defects over plate and plate-like structures. However, there is no effective SHM paradigm for small diameter pipes having salient curvatures. By utilizing GUW, we proposed three methods for SHM over pipes for different application backgrounds.

The first method detects the defect axial position. Measurements are acquired by our innovative dual transducer array design and are processed with the Multiple Signal Classification (MUSIC) signal processing method. The defect position is predicated accurately and efficiently, which is very adaptive for SHM over long pipes. However, it fails to predicate the defect circumferential position.

The second method detects both defect axial and circumferential positions. Measurements are acquired via the same transducer array setting as the previous method, and are processed by a novel method, Geodesic Distance MUSIC (GD-MUSIC) method, based on the assumption that the defect-reflected GUW only travels along the geodesic path embedded in pipe surfaces. It predicates the defect axial and circumferential positions accurately for single-defect cases. However, the detection accuracy is affected if it is applied to multiple-defect cases because the geodesic assumption does not hold,

which inspires us to design the third method.

The third method detects multiple defects as well as a single defect over pipes. After being acquired by the dual array setting, measurements are processed by an innovative statistical Predominant Component Voting MUSIC (PCV-MUSIC) method, which identifies defect locations on aggregation of a trove of inaccurate detection results. A pipe is unwrapped regarding different axial cuts to form different voters. Votes casted by voters are pipe images of voters obtained from MUSIC method. The polling result predicates both axial and circumferential defect positions even for multiple defects.

Finally, all methods are validated by multiple simulation cases.

ACKNOWLEDGMENTS

I would like to thank my committee chair, Prof. Sai Lau. This work could not have been done without his great advice and suggestions. In addition, I also would like to thank my committee members, Prof. Hamn-Ching Chen, Prof. Won-Jong Kim and Prof. Hong Liang (in the alphabetic order of last names) for their guidance on this research.

Thanks also go to Prof. Polycarpou, Prof. McAdams and staffs I have been working with for their support and help.

NOMENCLATURE

SHM	Structural Health Monitoring
GUW	Guided Ultrasonic Wave
MUSIC	Multiple Signal Classification
GD	Geodesic Distance
PCV	Predominant Component Voting
ANSI	American National Standards Institute
HAFEM	Hybrid Analytical Finite Element Method
SNR	Signal-to-Noise Ratio
EOM	Equation of Motion
DFT	Discrete Fourier Transform
FRF	Frequency Response Function
FFT	Fast Fourier Transfer
IRF	Impulse Response Function
NPRP	National Priorities Research Program

CONTRIBUTORS AND FUNDING SOURCES

Contributors

All work for the dissertation was completed independently by the student.

Funding Sources

This work was funded by Qatar National Research Fund under Grant Number NPRT 5-071-2-026.

TABLE OF CONTENTS

Page

LIST OF FIGURES

Page

LIST OF TABLES

Page

1. INTRODUCTION

1.1 Background

Structure Health Monitoring (SHM) [1] is applied in the area of structural defect detection for aerospace, civil and mechanical engineering infrastructure. It serves as an assessment for the penitential structural failure. Results obtained by SHM consists of detection, location and characterization of the structural damage [2]. Ultrasonic wave is one of the most popular tools for SHM over large-scale shell structures [3].

When an ultrasonic wave travels in a shell structure of which the thickness is smaller than or equal to the wavelength, this wave propagation is guided by the boundaries of the structure. Guided ultrasonic wave (GUW) can propagate a long distance with a low spatial decay, which enables applying GUW to SHM of large-scale shell structures [3][4].

GUW has two significant advantages in SHM applications. One is the short wavelength, which enables detecting small structural defects in a structure. The other is the long propagation distance, which reduces the number of measure locations when studying properties or detecting defects of a structure. The final goal of this research work is to accurately identify structural defects by GUW in small diameter cylindrical shell structures, such as gas and oil transportation pipes.

The knowledge of GUW propagation characteristics is required for its application in SHM. Compared to those of low frequency waves, GUW has rather complicated wave propagation characteristics. For lower frequency waves, cross-sectional mode shapes are independent of the excitation frequency. For GUWs, there are multiple mode

shapes at a single ultrasonic excitation frequency. These modes have different cross-sectional mode shapes and different wave speeds [5].

In a small diameter pipe, studied in this research, wave propagation characteristics of GUWs are even more complicated than those in flat shell structures such as plates. In plate structure, GUW modes can be divided into two types, symmetric wave modes and antisymmetric wave modes regarding the cross section of the plate. Especially, in the relative low ultrasonic frequency range, such as 10 kHz to 100 kHz, there are only two wave modes, *A*0 and *S*0, in plate structure. In small-diameter pipe there are three types of GUW, torsional, longitudinal and flexural waves. For each type of wave, there are multiple cross-section modes. Even in the relative low ultrasonic frequency range, 10 kHz to 100 kHz, there are multiple wave types and multiple wave modes for each wave type.

A conventional approach to overcome this difficulty is first to choose a wave type, which is less complicated to analyze such as axisymmetric torsional wave and longitudinal wave, which has less wave modes at low ultrasonic frequency range. Secondly, to choose a proper excitation method to reduce the frequency range of the excitation, so that the excitation is dominant by GUW with a specific cross-sectional mode. In practice, a customized ultrasonic transducer array is designed to generate the desired GUW excitation.

The SHM paradigm with GUW consists of two parts. The data acquisition part and defect visualization part. The data acquisition is about the measurement number, location and devices. The defect visualization part is about processing the measured

data with a signal processing method. When there are structural defects, excited GUWs are reflected from those defects. Defect-reflected GUWs are measured by ultrasonic transducer arrays. Features of defects can be extracted from analyzing these measurements.

1.2 Literature Survey

Ultrasonic wave has been gained interests in structure health inspection over pipelines as reviewed in [6][7][8]. The pulse-echo method [9] is a SHM paradigm that can be applied onto cylindrical pipes. In this method, one transducer generates an ultrasonic pulse and another transducer measures the defect-reflected wave referred as echoes. The location of the structural defect is calculated taking the time delays between the pulse and echoes as inputs. However, it is difficult to identify the size information of structural defects using this pulse-echo method. In addition, the pulse-echo method cannot be used to distinguish the boundary-reflected waves induced by structural discontinuities from defect-reflected waves. This conventional pulse-echo method was improved by adopting a time reversal process. A sensor array is introduced to suppress the boundary effects (or structural discontinuities) and thus increase the signal-to-noise ratio (SNR) of defect-induced signals [10]. The time reversal method has been widely applied for SHM of pipes [11][12][13]. However, the time reversal process requires undamaged baseline data that is difficult to obtain, in particular, for old structures existing before their SHM implementation. In [14], the common source method with a ring-type sensor array is used for SHM of cylindrical pipes. However, the spatial resolution of this method is limited by the aperture size of the sensor array.

The Multiple Signal Classification (MUSIC) beamforming method was first introduced by Schmidt [15] to locate multiple acoustic sources at a high spatial resolution. When structural defects are considered as passive sources, this MUSIC algorithm can be applied to visualize structural defects without the requirement of any undamaged baseline data. However, the conventional MUSIC beamforming algorithm is only suitable for the SHM of ideal shell structures, i.e., having infinite size and uniform thickness since defect-induced reflective waves are generally much weaker than waves reflected from any structural discontinuous features, such as rib-stiffeners or boundaries of non-ideal shell structures. In order to address this limitation, a time-frequency MUSIC beamforming algorithm was introduced in [16] and applied for the SHM of a plate.

However, an SHM paradigm with using the MUSIC method for plate is not suitable for small diameter pipes. When the diameter of the pipe is comparable to the wave length of the excitation GUW, GUW propagation characteristics over pipes cannot be simplified as those over plates, because the curvature of the circumferential area is not negligible. With the data acquisition system for plates, i.e., transducer array design, the MUSIC method cannot visualize the defect location at small diameter pipes.

When placed in a cylindrical coordinate frame, the defect location consists of two components, the axial location and the circumferential location. All previous SHM paradigms over pipe structure are designed to find the axial location of the defect. To detect the circumferential location of the defect on a small diameter pipe is even challenging compared to detect the axial location of the defect.

When GUW propagates along a small diameter pipe, we need to consider the circumferential distribution of particle displacements, i.e., angular profile [17]. It depends on the pipe dimensions, the excitation frequency and the propagation distance. When a defect presents, it introduces non-axisymmetric flexural modes. These non-axisymmetric modes interfere with axisymmetric torsional or longitudinal modes from the excitation. As a result, the exact prediction of the angular profile of the total field can only be realized by numerical methods. Compared with plate structures, this propagation character of GUW makes SHM more challenging for small diameter pipe structures. Angular profiles for large pipes were studied in [18]. It is shown that the large pipes have a natural focusing properties at certain axial locations, where the acoustic field was focused on a certain circumferential location. If it happens to be a defect, the defect reflected wave would be enhanced. Liu et. al. [19] provided a numerical method to identify the circumferential location of defects on small pipes based on [18] for the setting when the wave propagation cannot be simplified as a Lamb wave. However, in this method, baseline data were required to choose a proper excitation frequency, which is as high as 290 kHz.

Given the axial location of defect and defect-free baseline data, the circumferential location of the defect can be identified in [20],. Deng et. al. obtained the baseline data by placing a measurement sensor array at the axial location of detect. Compared measurements from the defected pipe and the baseline pipe, the circumferential location of the defect was identified. [21] and [22] showed that by applying a tuned phase angle to each transducer in the excitation transducer array, the acoustic field could be focused

at the certain location. That focusing method increased the chance to detect defects. However, this method is only suitable when the location of the defect is confined within a small region. It is inefficient for scanning a large area. In [23], transducers in the array is fed with different excitations. These excitations have different amplitudes and time-delays. The energy generated by this transducer array can be successfully focused at any predetermined locations in pipes. In a circumferential scan, the maximum amplitude of the defect echo was recorded and then plotted with respect to each focal angle. This produces an experimental angular profile of the reflected wave. The theoretical angular profiles of the reflected wave are obtained by calculating the focused guided wave energy impinged onto defects with different cross sectional areas. By comparing theoretical and experimental profiles, the circumferential extent of the defect can be effectively measured. This method requires baseline data from the theoretical angular profile.

Besides focusing methods for the defect detection in circumferential location, [24] developed an algorithm based on two-dimensional (2-D) blind deconvolution. A circumferential guided wave array was built for sending and receiving guided waves along the pipe. All transducers in the array were connected to a single channel pulsar/receiver through multiplexers. The guided wave echoes acquired by the multiplexed circumferential transducer array are processed for evaluating circumferential distributions and geometry of the defects. This method also required the angular profile at the axial location of the defect. In [25], the defect location in the circumferential direction was detected, by moving two transducers along the

circumferential direction. This method is only applicable for large diameter pipes with thick walls.

1.3 Problem Statements

There are different criteria to decide whether a pipe can be considered as a large pipe or a small pipe. In [18], a pipe is considered as a large pipe when the pipe wall thickness is far less than the cylinder diameter and the wavelength is smaller than or comparable to the pipe wall thickness. In [26], when the diameter of a pipe is smaller than 50 mm, it is considered as small pipes. In large pipes, the acoustic field can be analysed based on the characteristics of Lamb waves [27] that travel along a periodic unwrapped plate. In small pipes, the GUW cannot be simplified as a Lamb wave.

We considered a pipe as a small diameter pipe, when the radius of a pipe is comparable to the wavelength of the chosen GUW excitation. SHM for the small diameter cylindrical shell structures is more complicated than that for plate structures, because of complex GUW wave propagation properties in small diameter cylindrical shell structures. Plane-directional wave components of the GUW propagating in an isotropic plate are similar in their wave propagation properties. However, in the small diameter structures, GUW propagation properties are directional due to the different curvatures in the axial and the circumferential directions. Those directional GUW propagation properties make it difficult to generalize acoustic imaging methods so that they can be applied to both the plates and the highly curvature cylindrical shell structures. In addition, due to the small diameter of the interested pipe, the number of transducers in the circumferential direction is limited, which reduces the spatial

resolution of the structural defect image in the circumferential direction.

The problem we want to address is how to design a SHM paradigm for small-diameter pipes. This SHM paradigm should generate a high spatial resolution pipe image, in which both axial and circumferential locations of the defect can be revealed simultaneously at a relative low frequency. This problem can be break into three smaller problems.

The first problem we want to address is, given the fact that GUW propagation is complicated in small diameter pipes, how to generate a proper GUW excitation. This problem can be further decomposed into two parts, what is the proper GUW excitation and how to generate the desired GUW. To generate a proper GUW, we need to choose the excitation mode and frequency. The excitation mode is decided by types of applications. For example, if the pipe is filled with fluid, the longitudinal excitation is not suitable since the fluid affects the longitudinal wave propagation characteristics [28]. For the excitation frequency, GUW with higher frequency is more sensitive to small defects, but it also requires smaller spacing in the transducer, which is limited by the physical constrains such as dimensions of transducers. Once the excitation is chosen, a transducer array need to be designed to generate the expected excitation.

The second problem is how to design the data acquisition system. As mentioned before the MUSIC signal processing method gives a high spatial resolution pipe image, on which the defect location is revealed. However, MUSIC method cannot be applied onto small-diameter pipes with existing data acquisition system. A new transducer array design is required for the data acquisition system, so that this high special resolution

signal processing method can be applied onto small diameter pipes.

The third problem is how to design a signal processing method to extract both the axial and circumferential defect location. In the MUSIC method, the propagation path of the defect-reflected wave is an essential information for defect visualization. However, for defect-reflected GUW, its propagation path in the circumferential direction is unknown. As a result, the traditional MUSIC method only provides the axial location information of the defect. New signal processing methods, in which the defect-reflected wave propagation path is corrected modelled, must be developed for detection of the circumferential location of the defect.

An experiment schema is also needed for validation of the proposed SHM paradigm. However, a set of existing commercial equipment (in particular, the transducer array and its holder) cost more than $10K [29], which is unaffordable by our research funding. Additionally, those types of commercial equipment are optimized to specific SHM applications, they are not customizable, and are not compatible with other ultrasonic data acquisition systems (DAQ) or transducers.

1.4 Objectives and Approaches

Objectives of this research, aiming to address previous issues, include (1) Design an ultrasonic transducer array to generate GUW excitation with a desired wave mode; (2) Design the measurement transducer array for the data acquisition; (3) Design a high spatial resolution signal processing method to visualize the circumferential location of the detect as well as the axial location of the defect at the same time with a relative low frequency excitation.

These objectives have been achieved by using the following approaches. First, the GUW propagation properties are studied by generating the dispersion curves of various GUW modes, which provide the information on (1) GUW cross-sectional modes that are excited at a specific frequency, (2) GUW cross-sectional mode shapes that can be used to develop a specific excitation method, and (3) the wave speed of each GUW cross-sectional mode. Those information are essential for choosing the GUW cross-sectional mode and the excitation frequency, and for designing the ultrasonic transducer array.

The data acquisition system is designed by choosing the proper measurement location (transducer array location) and the number of measurements (transducer array configuration). The measured data is used for signal processing to extract the feature of the defect. We first demonstrate that with the proposed novel transducer array design, the axial location of the defect can be detected with high accuracy on an ANSI 1½ inch pipe with 30 kHz $T(0,1)$ GUW excitation. However, this method cannot detect the circumferential location of the defect because of the uncertainty in the defect-reflected GUW propagation path.

Two novel signal processing methods are developed to work with this data acquisition system. In this first method, GD-MUSIC method, it is assumed that the defect-reflected GUW propagates along the geodesic path over the 3-D cylindrical pipe surface. This method correctly extracts the circumferential location as well as the axial location of the defect from the measurements. However, the geodesic propagation path assumption does not hold for multiple defects.

In the second method, PCV-MUSIC method, the uncertainty of the defect-

reflected GUW is eliminated by a statistic method. The pipe is unwrapped with respect to different axial cuts, referred as voters. The defect location on each unwrapped case is different. The defect-reflected GUW is assumed to travel along the Euclidean path on the 2-D unwrapped pipe surface. The MUSIC power result based on this assumption is generated for each unwrapped case, referred as vote. All votes are combined by mapping and summation to form the final result of the pipe image, in which both axial and circumferential locations of the defect is correctly revealed.

Note that the proposed method is suitable but not limit to a specific excitation mode or frequency. The detailed configuration of the transducer array, such as the number of transducers in the transducer array, might be different when the excitation is different, but the paradigms are still applicable.

1.5 Brief Overview of Sections

Below is the structure of this dissertation thereafter.

Section 2 presents criteria for choosing proper excitation for SHM, and transducer array design for generating the desired excitation. The dispersion curves, which represent the wave speed as a function of frequency, are generated for all the axisymmetric mode within the frequency range 10 kHz to 100 kHz. Dispersion curves provide the information which is need to choose the GUW mode and frequency for excitation. In this section, two different methods are presented to generate dispersion curves for cylindrical pipes. One is an analytical method, which is applicable when the material of the pipe is homogenous. The other is a hybrid method, which has more general application even when the pipe has coating or is filled with fluid.

Section 3 focuses on visualizing the axial defect location. Two transducer array designs are presented. When the excitation is non-GUW, the number of measurements linearly increases with the length of the interested pipe. Since the non-GUW has one dimensional propagation characteristic, the pipe is also abstracted as a 1-D system. When the excitation is a GUW, measurements are collected by a dual transducer array system. When the defect is located within the region bounded by dual transducer arrays, the axial location of the defect can be detected with high accuracy.

Section 4 adopts the dual transducer array setting for the measurement data acquisition. Two new data processing methods are presented to identify the defect location in both axial and circumferential directions. One is GD-MUSIC method, in which the defect-reflected wave is assumed to propagate along the geodesic path embedded in the 3-D cylindrical surface of the pipe. In single defect cases, this method correctly detects the circumferential location of the defect as well the axial location of the defect with 50 kHz GUW excitation. The other is PCV-MUSIC method, in which the location of the defect is voted by different voters, which are formed by unwrapping pipe regarding different axial cuts. Besides visualizing single defect, this method can also visualize circumferential and axial locations of multiple defects.

In Section 5, the recommended experiment schema is presented to validate proposed SHM paradigms. The device selection, experimental setup and experiment procedure are presented. The number and dimensions of transducers are decided by sizes of interested pipes. A transducer gripper is designed to mechanically couple the transducers with the pipe. The design is validated in simulation over a finite element

model and its prototype is printed out using a 3D printer. The experimental setup, which includes the choice of the NI modular, is presented. The LabVIEW script design is also presented.

2. GUW PROPAGATION CHARACTERISTICS IN CYLINDRICAL PIPES

GUW propagation characteristics are studied by generating its dispersion curves. A dispersion curve is a numerical model describing the relation between the wave speed and the frequency [5]. It provides knowledge to choose the proper excitation GUW mode and frequency for SHM over an interest pipe structure. For pipes made of homogenous material, dispersion curves of GUW is obtained by solving the analytical eigenvalue problem presented in [5]. For pipes with coating or filling with water, dispersion curves of GUW are obtained by the Hybrid Analytical/Two-Dimensional Finite Method (2D HAFEM) [30][31]. In general, GUWs propagating in pipes are classified into three types: flexural, longitudinal, and torsional waves. For simplicity of statements, each wave mode is denoted in the form $X(n, m)$, where X is the wave type, n is the circumferential order, and m is the wave mode number. Meanwhile, we denote the longitudinal mode by L and the torsional mode by T. For torsional and longitudinal waves, which are axisymmetric, their circumferential orders n, are both zero. For flexural waves, which are not axisymmetric, have different circumferential orders denoted by integer n. All three wave types have different mode numbers denoted by positive integer m. As the excitation frequency increases, more GUWs with different cross-sectional modes are excited at a single excitation frequency.

In following subsections, we briefly reviewed the analytical method and HAFEM for obtaining dispersion curves of GUWs propagating over pipes we interested. Based on the dispersion curves, the proper GUW mode and frequency are chosen as excitation for simulation and experimental schema design. Meanwhile, the robustness of the

chosen GUW mode is validated by the sensitivity analysis.

2.1 Analytical Method for GUW Dispersion Curves

When GUW propagates over pipe structure, the EOM of solid particles of the structure is described by Navier governing equation. When the particle displacement vector is expressed by expansion penitential and rotation potential, the wave equation of this GUW is derived from the Navier governing equation. The boundary condition for this wave equation is traction-free boundary conditions, which stands when there is no external force applied. Together with the boundary conditions, the dispersion relation will be formed as an eigenvalue problem, in which the relation of wave speed and frequency are provided implicitly.

Dispersion curves of GUWs depend on the dimension of the material properties of the structure, over which GUWs propagate. In this subsection two types of pipes are considered. One of them is American National Standards Institute (ANSI) 1½ inch (outer diameter is 4.82 cm) schedule 5 (thickness is 0.165 cm) [32]. The other pipe is ANSI 4 inch schedule 5. Both of them are made of stainless steel 304. These two types of pipe are considered because, in the following sections, they will be served as benchmark simulation models, over which the proposed paradigms are validated.

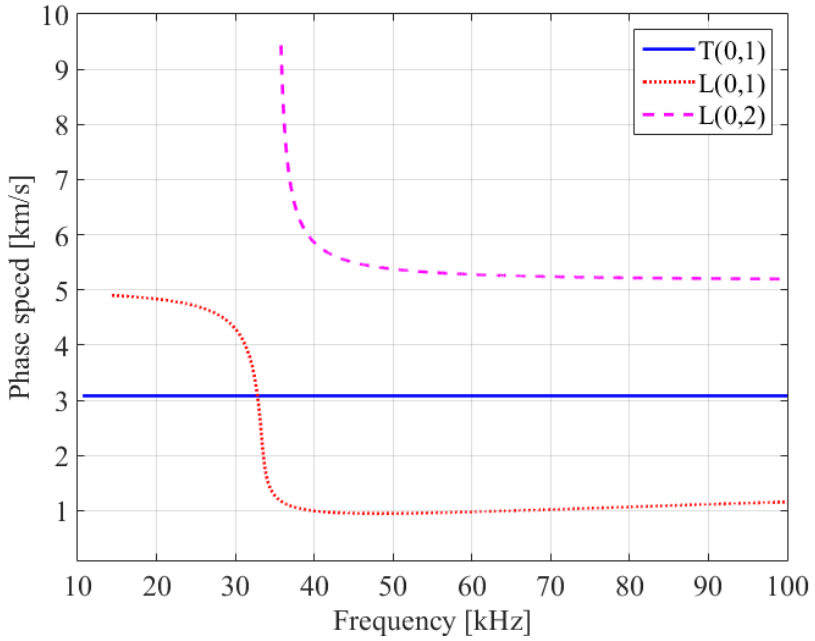

Figure 1. Dispersion curves of ANSI 1½ inch schedule 5 pipe with outer diameter of 4.82 cm and thickness of 0.165 cm.

By applying this analytical method over this stainless steel pipe, we obtain three dispersion curves of the axisymmetric GUW modes propagating over this pipe, as shown in Figure 1. Those three curves describe three axisymmetric wave modes existing within the frequency range between 10KHz to 100KHz. Two longitudinal wave modes $L(0,1)$ and $L(0,2)$ are indicated by a red dotted line and a magenta dashed line respectively. One torsional wave mode, $T(0,1)$, is indicated by the blue line. Only the axisymmetric modes of GUW are considered here because they can scan the whole pipe avoiding any blind spots.

Geometry shapes of dispersion curves imply physical properties of GUW. The torsional wave mode has the advantage over longitudinal wave: 1) there is only one

torsional mode with the frequency range. There is no double mode conversion phenomenon which introduces extra echoes and leads to wrong defect inspection results [33]; 2) the dispersion curve of *T*(0,1) is a straight line, which means that the wave phase speed is a constant. This constant wave speed simplifies the SHM procedure significantly, because the echo from the defect only depends on the distance when the wave propagation speeds is constant. Furthermore, *T*(0,1) mode is generally more preferable to longitudinal mode because the employed transduction system is simpler and lighter [34]. In addition, in liquid filled pipes, longitudinal excitation tends to have poorer SNR. Because of those reasons, *T*(0,1) GUW is the best excitation wave mode among three modes for the structural inspection of this ANSI 1½ inch schedule 5 pipe.

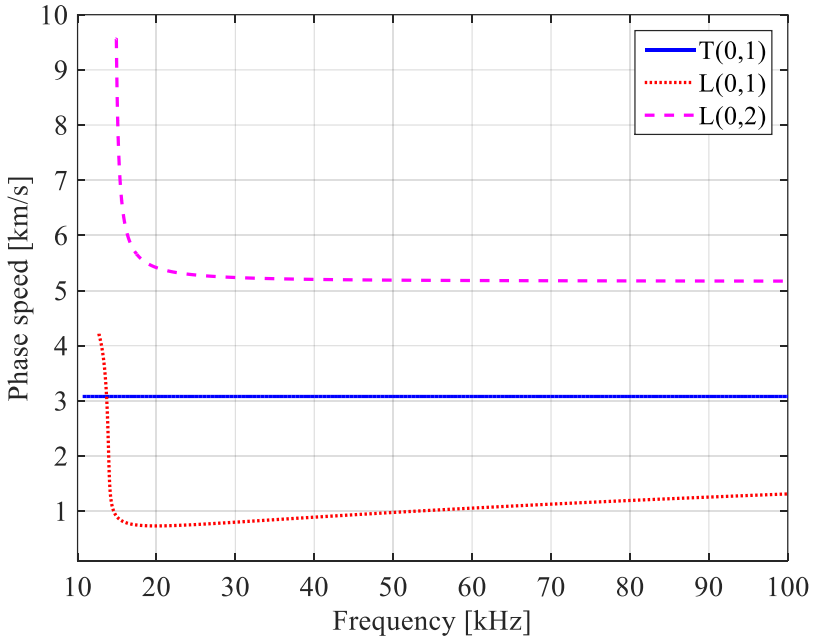

Figure 2. Dispersion curves of ANSI 4 inch schedule 5 pipe with outer diameter of 11.43 cm and thickness of 0.21 mm.

Another dispersion curve result by applying the analytical method over an ANSI 4 inch schedule 5 pipe is shown in Figure 2. We will revisit this type of pipes in Section 4. Similarly, there are three dispersion curves within the frequency range 10 KHz to 100 KHz. The dispersion curve of the axisymmetric torsional mode, $T(0,1)$, is indicated by a blue solid line. The other two axisymmetric longitudinal mode, $L(0,1)$ and $L(0,2)$ are indicated by red dotted line and magenta dashed line, respectively. As the ANSI 1½ inch schedule 5 pipe, there are two longitudinal waves of $L(0,1)$ and $L(0,2)$, and only one torsional wave of $T(0,1)$ exists in the frequency range of 10KHz to 100KHz. The reasons for choosing $T(0,1)$ as excitation GUW mode still stands for this case.

Note that the dispersion curves of longitudinal modes, $L(0,i)$, $i = 1, 2$, changes regarding changes of pipe dimensions. However, for the torsional wave T(0,1), two different pipes share a same torsional dispersion curve.

2.2 Sensitivity Analyses

Based on the discussion over the analytical method, the dispersion curve of $T(0,1)$ is invariant for two different pipe dimensions. By introducing more pipe models, we study factors of pipe that affect the dispersion curve, i.e., we study the sensitivity of $T(0,1)$ dispersion curve when propagating over different pipes.

When GUW propagates over homogeneous material pipes and the material is the same for all the interested pipes, shapes of dispersion curves are only affected by cross-section dimensions of the pipe. The outer diameter and the thickness are the only two components of cross-section dimensions of a cylindrical pipe. We studied the sensitivity of $T(0,1)$ to those two components by comparing the dispersion curves of $T(0,1)$.

Models are still simulated within frequency range from 10 kHz to 100 kHz. For simplicity, we name a pipe *small diameter* pipe if the diameter of this pipe is comparable or smaller to the excitation wavelength of GUW. For example, ANSI 24 inch pipe (radius of 0.305 m) is considered as a small diameter pipe to the GUW with wavelength as 0.307 m. The ANSI 24 schedule 5 pipe is adopted to show how the diameter of the pipe effects the dispersion curve of $T(0,1)$.

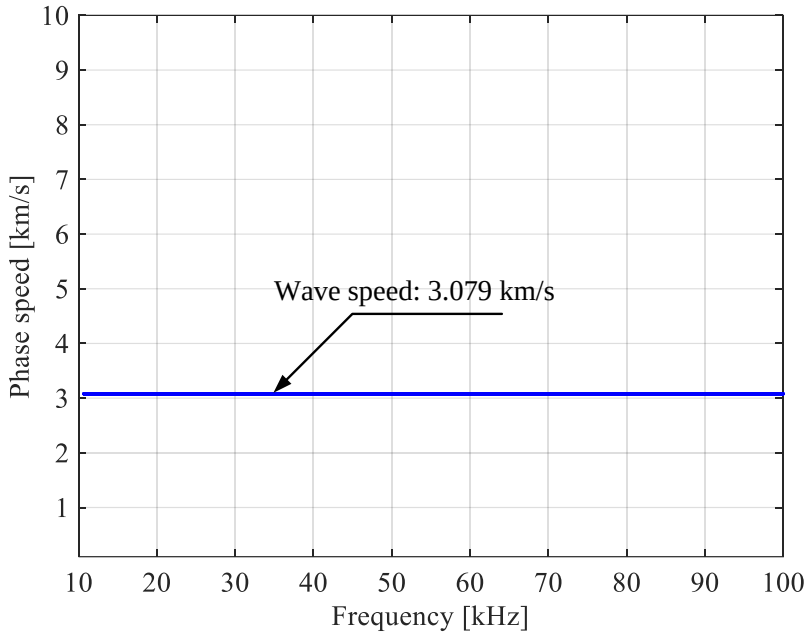

Figure 3. Dispersion curve of axisymmetric torsional wave *T*(0,1) for ANSI 24 inch schedule 5 pipe.

By applying the analytical method to the pipe model, we obtained the dispersion curve of T(0,1) for ANSI 24 inch schedule 5 pipe in Figure 3. As shown in Figure 3, when propagating over this pipe, the axisymmetric torsional mode $T(0,1)$ has the same

dispersion curve as propagating over the ANSI 1½ inch schedule 5 pipe. In other words, when the wave speed of $T(0,1)$ does not changes when propagating over pipe of different diameters.

So far, the pipes considered in this research are all ANSI schedule 5, which is also the smallest wall thickness in ANSI standard. However, the thickness of the wall is also a component that could affect the shape of dispersion curves. In Figure 4, the ANSI schedule 40 is chosen to study the sensitivity of $T(0,1)$ regarding the thickness of pipe wall. ANSI schedule 40 is chosen because it is the standard thickness for pipes.

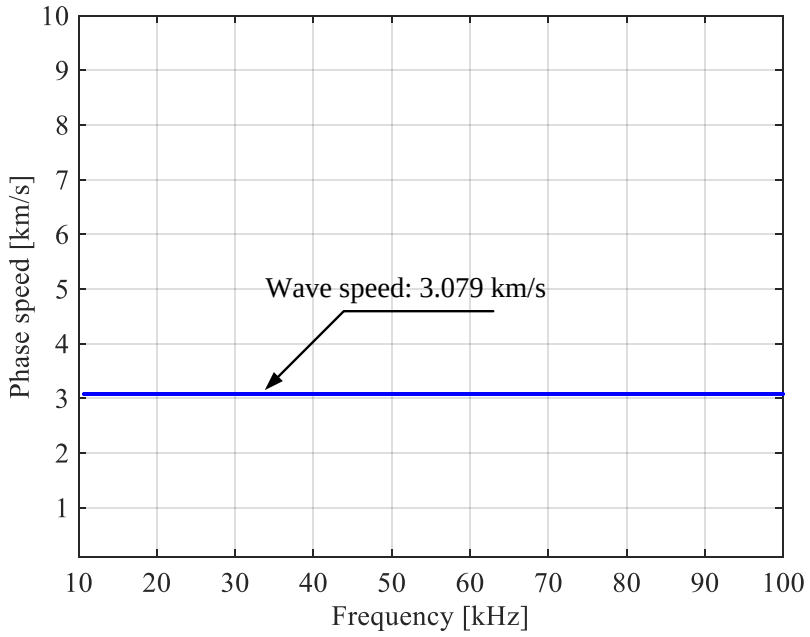

Figure 4. Dispersion curve of axisymmetric torsional wave *T*(0,1) for ANSI 4 inch schedule 40 pipe.

Figure 4 shows the dispersion curve of $T(0,1)$ over an ANSI 4 inch schedule 40

pipe. Compared with previous cases, the dispersion curve of $T(0,1)$ is not changed regarding the change of the pipe wall thickness. The wave speed of the axisymmetric torsional wave $T(0,1)$ is the same as the schedule 5 pipes, which is still 3.079 km/s. As a conclusion, the wave speed of axisymmetric torsional wave $T(0,1)$ is not sensitive to the thickness and outer diameter of the pipe. In other words, the $T(0,1)$ has the same wave speed when propagates along different size of pipe.

2.3 Hybrid Method for GUW Dispersion Curves

The limitation of a pure analytical method is that it is only suitable for the pipe with homogeneous material. If the pipe is filled with water or coated with different materials, a pure analytical method is no longer applicable. The dispersion curve changes when the material changes. The interaction between materials cannot be found by analytical method. For these settings, one solution to calculate the dispersion curves is to use a numerical method, such as finite element method (FEM) [35]. The interaction between different material is calculated by discretion and approximation.

In particular, for waves in ultrasonic frequency range, the wave length is small, so a large number of finite elements are required for ensuring the computing accuracy in study of wave propagation characteristics. Two-Dimensional Hybrid Analytical Finite Element Method (2-D HAFEM) presented in Ref. [30] provides a method to reduce the computation cost by an approximated model. In this method, the traditional FEM is applied on the cross-section area of the pipe and an analytical solution is assumed in the axial direction.

The HAFEM is briefly reviewed here and the detail information is in Ref. [30]. In

HAFEM, the equation of motion (EOM) of each node is

$$\mathbf{K}_{zz}\frac{\partial^2\mathbf{u}}{\partial z^2}+\mathbf{K}_{(\xi+\eta)z}\frac{\partial\mathbf{u}}{\partial z}+\mathbf{K}_{\xi+\eta}\mathbf{u}+\mathbf{M}\frac{\partial^2\mathbf{u}}{\partial t^2}=\mathbf{f}^{\mathrm{e}}, \tag{2.1}$$

where **u** is the vector of the nodal displacements in the cross-section area. It is a function of the axial location *z*. When the pipe length is infinite in the *z*-direction, there is no reflected wave in axial direction. **K** matrices are obtained from the variation principle of the energy method [35]. These matrices are only related to material properties of the object and the finite element model of the cross section area. The **M** matrix is the mass matrix. f_e is the external force that applied to nodes. The nodal displacement can be represented as a propagating wave without any reflection as

$$\mathbf{u}=\mathbf{u}_0\mathrm{e}^{\mathrm{j}(kz-\omega t)}, \tag{2.2}$$

where k is the wave number and ω is the angular frequency, and where j is the imaginary unit. By plugging Eqn. (2.2) into Eqn. (2.1), an eigenvalue problem is obtained, as

$$\left(-\mathbf{K}_{zz}k^2+\mathrm{j}k\mathbf{K}_{(\xi+\eta)z}+\mathbf{K}_{\xi+\eta}-\omega^2\mathbf{M}\right)\mathbf{u}_0=0.$$

In order to have a non-trivial solution, the determinant of the coefficient matrix should be zero. Thus, there is

$$\det\left(-\mathbf{K}_{zz}k^2+\mathrm{j}k\mathbf{K}_{(\xi+\eta)z}+\mathbf{K}_{\xi+\eta}-\omega^2\mathbf{M}\right)=0,$$

where det(.) is the determinant of a matrix. The solution of this eigenvalue problem gives the dispersion relation between the wave phase speed c_p and the frequency f.

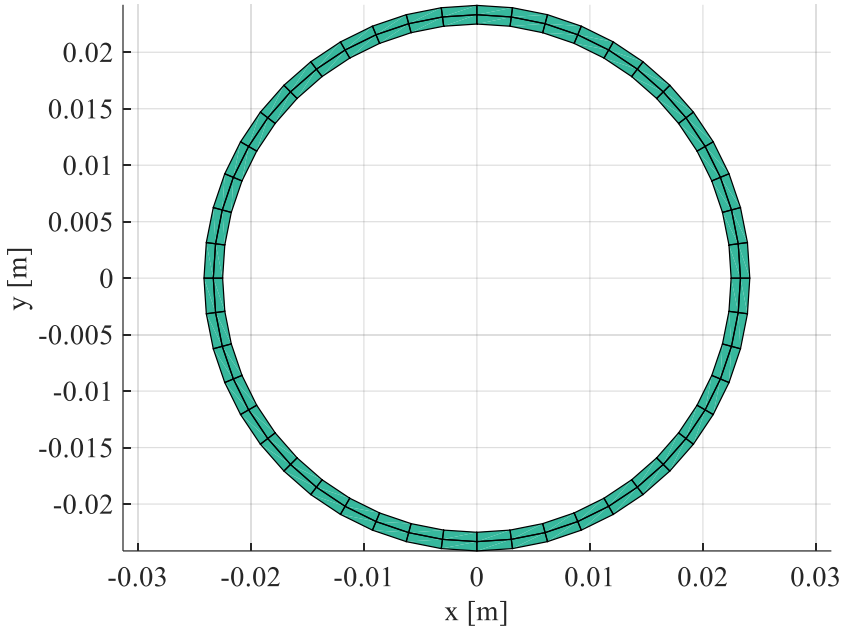

Figure 5. FE mode of the cross-section area of ANSI 1½ inch schedule 5 pipe.

Figure 5 illustrates the 2-D HAFEM model of the same 1½ pipe of which the dispersion curve is studied by analytical method in Figure 1. The 2-D FE model is built for the cross-section area. In this 2-D FE model, the quadratic 2-D element is chosen. There are 9 nodes in each element. There are 2 elements in the radial direction and 48 elements in the circumferential direction. According to Nyquist sampling criteria [36], the mesh size should be less than half of the excitation wavelength to avoid alias in analysis of the wave propagation characteristics. In this case, the maximum node spacing is 1/311 of the wavelength of $T(0,1)$ at 100 kHz.

The FE method is applied to the cross section area, while the analytical wave propagation model is applied in the axial direction. This reduces the computation cost in the axial direction. When the pipe has different layers, such as coating, in r-direction,

the cross-section FE model for the cross section area will be changed based on the material and thickness of each layer.

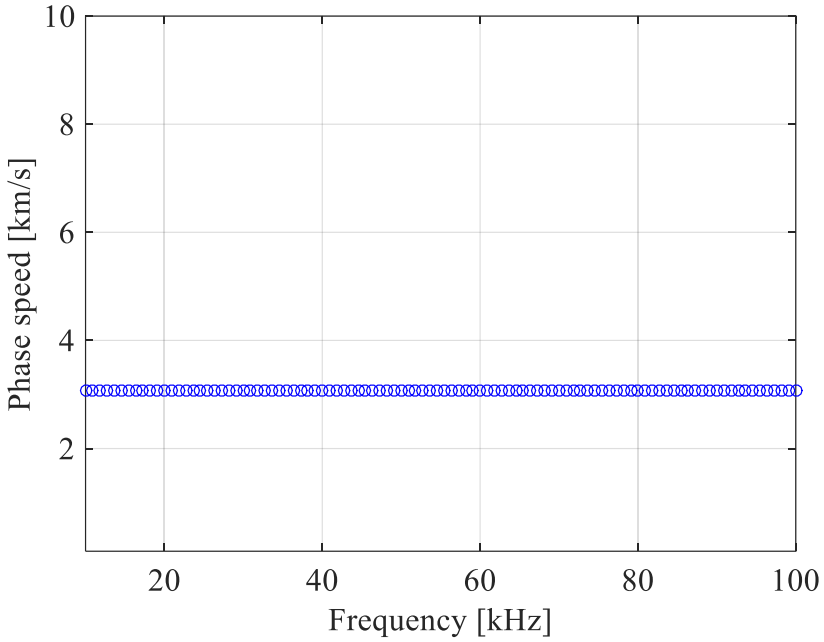

Figure 6. Dispersion curve of *T*(0,1) for ANSI 1½ inch schedule 5 pipe obtained from 2-D HAFEM.

Figure 6 shows dispersion curves obtained with the 2-D HAFEM method. The result of the dispersion curve is the same as the analytical result (shown in Figure 1). Therefore, HAFEM method is validated by this simulation. The advantageous of HAFEM method are it is applicable to non-homogenous material pipe with less computation cost compared to a full 3-D FEM. However, the existing 2-D HAFEM is not applicable for the pipe with structural defects. For pipes with structural defects, the wave propagation in axial direction cannot be obtained analytically due to its geometry and the reflected wave introduced by the defect. As a result, for the simulation cases

presented Section 3 and Section 4 are all built as a full, three-dimensional (3-D) FE model, of which the computation cost is high for the simulations. That's why all FEM computations are processed on supercomputers.

2.4 Transducer Array Design

As mentioned in Section 2.1, $T(0,1)$ is chosen as the excitation mode. There are two ways to generate this desired axisymmetric torsional wave mode. One is to use a single shear transducer in the ring shape to be assembled at the outer surface of the pipe as a collar. Single transducer is easy to excited and only need one channel for the input signal. The disadvantage of this method is the size of this transducer is not configurable. One transducer can only be used for pipes with the same outer diameters. The other method is to use a shear transducer array consisting of N transducers, which are evenly distributed around the outer surface of a pipe in circumferential direction. The transducer array is configurable to different size pipes by changing transducer numbers or spacing. Additionally, the transducers in the transducer array can also serve as measurements to measure the echoes from defect or the end of the pipe. The disadvantage of this method is each transducer should be exactly the same to generated the complete axisymmetric excitation. More input changes are also required to fire all the transducers at the same time.

The ultrasonic transducer array configuration is designed based on the chosen GUW mode. In order to satisfy the Nyquist sampling criterion, the spatial sampling space between two adjacent ultrasonic transducers should be smaller than a half of the excitation wavelength. At low frequencies, the $T(0,1)$ wave has a relatively long

wavelength. In this case, it requires a small number of ultrasonic transducers, which reduces the structural inspection complexities and expenses significantly, while allows to detect only relatively large structural defects.

In Section 3, 30 kHz is chosen as the excitation frequency for ANSI 1½ inch schedule 5 pipe, of which the corresponding wavelength is 10.2 cm based on the dispersion curve of $T(0,1)$. In consideration of the outer pipe diameter of 4.82 cm, eight transducers are placed around the pipe equally on the pipe circumference to generate the axisymmetric $T(0,1)$ excitation. The sampling space is 1.9 cm, which is less than a quarter of the excitation wavelength, which satisfies the Nyquist sampling criterion. The transducer dimensions are selected as 7 mm by 7 mm with a thickness of 5 mm. When applied with a sinusoidal excitation voltage at the frequency of 30 kHz, all the transducers synchronously generate the shearing vibration motion of the $T(0,1)$ wave in the circumferential direction. This transducer design is also chosen for the experiment design in Section 5.

In Section 4, 50 kHz is chosen as the excitation frequency for ANSI 4 inch schedule 5 pipe, of which the corresponding wavelength is 6.15 cm based on the dispersion curve of $T(0,1)$. The outer diameter of the pipe is 11.42 cm. At least 12 transducers are required in the circumferential direction to meet requirement of the Nyquist sampling criterion.

2.5 Conclusions

There is no explicit analytical form for the relation between frequencies and wave speeds of GUWs propagating over a small diameter pipe. Dispersion curves provide a

numerical way to demonstration these relations. There are two ways to calculate the dispersion curves, the analytical method and HAFEM. The later one has boarder applications including the pipe composite of different materials in cross-section areas. Axisymmetric dispersion curve $T(0,1)$ is chosen as the excitation mode because it is the only axisymmetric torsion mode in the frequency range from 10 kHz to 100 kHz. Furthermore, its constant wave speed simplifies the signal processing procedure. The ultrasonic transducers are chosen to generate the axisymmetric shear motion. The spacing of transducers satisfies the Nyquist Sampling criteria. The sensitivity analysis also shows that the dispersion curve of $T(0,1)$ is not sensitive to dimension changes of the pipe, which also simplifies the process for SHM for pipes of different sizes.

3. STRUCTURAL DEFECT IDENTIFICATION: AXIAL LOCATION*

Though it detects structural defects of plate structures in Ref. [16], this SHM method is not applicable to small diameter pipe with the existing data acquisition system. That is because the GUW propagation characteristics over small diameter pipes are different from that over plates, as explained in Section 1. However, the signal processing method presented in Ref. [16] inspires us to design a similar method for processing measurements on small diameter pipes.

In this section, the axial defect location is visualized over pipe structures with both non-GUW excitation and GUW excitation. A case with a non-ultrasonic frequency excitation is first presented to demonstrate that, with enough measurements, the axial location of the defect can be correctly visualized. To reduce the number of measurements, the second case, with $T(0,1)$ GUW excitation, is then presented to demonstrate that, with a creative data acquisition system the axial defect location can be correctly visualized. Both cases are validated by simulations

3.1 MUSIC Signal Processing Method

This section introduces the theory background of Multiple Signal Classification (MUSIC) method and Time-Frequency MUSIC (TF-MUSIC) method. Both methods serve as a part of SHM paradigms to process the measurement signal and generate the

* Portions of this section have been reprinted with the permission of Institute of Noise Control Engineering, from S. Jiang, M. Karkoub, and Y.-J. Kim, "High-Resolution Ultrasonic NDE Imaging Method with Virtually Expanded Circumferential Aperture in Small-Diameter Cylindrical Oil/Gas Pipes," *INTER-NOISE and NOISE-CON Congress and Conference Proceedings*, **252(2)**, 174-183, 2016. [37]

pipe image, on which defect locations are visualized.

3.1.1 MUSIC Method

The MUSIC method is a signal processing method proposed by R. Schmidt in Ref. [15]. The received signal on a transducer array is processed in frequency domain to estimate the source locations.

Assume there are M transducers forming a transducer array. The time domain measurement of the m-th transducer is denoted as $x_m(t)$. t is discrete time data. Applying Discrete Fourier Transfer (DFT), we obtained the frequency spectrum of time domain measurement $x_m(t)$, denoted as $X_m(f)$. The frequency spectrums from all M transducers form a vector $\mathbf{X}$. At a specific frequency f_l, $\mathbf{X}$ has the forms as

$$\mathbf{X}(f_l) = [X_1(f_l)\ \ X_2(f_l)\ X_3(f_l) \cdots X_M(f_l)]^{\mathrm{T}}\ , \tag{3.1}$$

where the subscript l is the frequency index and the superscript T is the transpose of a matrix or vector.

The cross-spectrum analysis is applied to all the measurements. The M by M cross-spectral matrix $\mathbf{R}$ at frequency f_l is obtained by

$$\mathbf{R}(f_l) = \mathbf{X}(f_l) \cdot \mathbf{X}^{\mathrm{H}}(f_l), \tag{3.2}$$

where the superscript H represents the Hermitian transpose of a matrix or vector.

The cross-spectrum matrix $\mathbf{R}(f_l)$ is decomposed by the Singular Value Decomposition (SVD) and represented as

$$\mathbf{R}(f_l) = \mathbf{U}(f_l)\mathbf{\Sigma}(f_l)\mathbf{V}^{\mathrm{H}}(f_l). \tag{3.3}$$

The structure of interested is discretized and represented by a set of scanning points. Assume the total number of scanning point is N. In 3-D Cartesian coordinate system, n-th scanning point, S_n, is represented by its coordinates, (x_s, y_s, z_s).

The MUSIC method result, MUSIC power, is a function of the scanning point location and frequency. At scanning point S_n and frequency f_l, MUSIC power, $P_{MUSIC}(f_l, S_n)$ is defined as

$$P_{\mathrm{MUSIC}}(f_l, S_n) = \frac{1}{\sum_{i=p+1}^{M} \left| \mathbf{g}^{\mathrm{H}}(f_l, S_n) \cdot \mathbf{u}_i(f_l) \right|^2}, \tag{3.4}$$

where p is the dimension of the signal subspace. $\mathbf{u}_i$ is the i-the column of the matrix $\mathbf{U}(f_l)$ is Eqn. (3.3). $\mathbf{u}_i$, $i = p+1, \cdots, M$, represents the noise subspace of the measurements. $\mathbf{g}(f_l, S_n)$ is referred as steering vector. It represents the spatial distribution of the signal power at the measurement locations when a free-field point source is placed at the scanning point S_n. $\mathbf{g}(f_l, S_n)$ has the form

$$\mathbf{g}(f_l, S_n) = [\mathrm{e}^{jk(f_l)r_1(S_n)} \quad \mathrm{e}^{jk(f_l)r_2(S_n)} \quad \cdots \quad \mathrm{e}^{jk(f_l)r_M(S_n)}]^{\mathrm{T}} \tag{3.5}$$

where j is the imaginary unit. $k(f_l)$ is the wave number of the signal at frequency f_l. $r_m(S_n)$ is the distance of the wave propagation path from the scanning point S_n to the m-th measurement. If the wave propagates along the Euclidian shortest path, there is

$$r_m(S_n) = \sqrt{(x_m - x_n)^2 + (y_m - y_n)^2 + (\mathrm{z}_m - z_n)^2}, \tag{3.6}$$

where (x_m, y_m, z_m) is location of m-th measurement in 3-D Cartesian coordinate system.

ere $r_i = \sqrt{(x_i - x_s)^2 + (z_i - z_s)^2}$ is the distance between the *i*-th transducer (x_i, z_i) and a scanning location (x_s, z_s).

The image of the scanning area is obtained when the MUSIC power is treated as colormap at each scanning point. The MUSIC power reaches its maximum value, when the scanning point is the actual source of the field. As a result, the source can be identified on the image of the scanning area.

3.1.2 Time-Frequency MUSIC Method

The MUSIC method has a variation referred as time-frequency MUSIC (TF-MUSIC) method by A. Belouchrani in Ref. [38]. TF-MUSIC method adds the time information to MUSIC method. Music power obtained from TF-MUSIC method changes regarding time.

In TF-MUSIC method, the time domain measurement of the *m*-th transducer, $x_m(t)$, is divided into multiple time segments. For each time segment, there is supposed to include at most one event, such as the direct excitation, defect reflection, or the boundary reflection. Each time segment is turned by a time window. To avoid information loss, the overlapping is added between two adjacent time segments.

The q-th time segment, which stars at $t_{q,s}$ and ends $t_{q,e}$ is denoted as $x_{m,q}(t)$, $t_{q,s} < t < t_{q,e}$. The frequency spectrum of measurement of q-th time segment is denoted as $X_m(f_l, t_q)$, where t_q is the median time point of q-th time segment.

The frequency spectrums from all M measurement form for q-th time segment at frequency f_l is

$$\mathbf{X}(f_l,t_q)=[X_1(f_l,t_q)\ \ X_2(f_l,t_q)\ \cdots\ X_M(f_l,t_q)]^{\mathrm{T}}\ , \tag{3.7}$$

The cross-spectrum matrix at frequency f_l is obtained by

$$\mathbf{R}(f_l,t_q)=\mathbf{X}(f_l,t_q)\cdot\mathbf{X}^{\mathrm{H}}(f_l,t_q)\,, \tag{3.8}$$

where the superscript H represents the Hermitian transpose of a matrix or vector.

The SVD decomposition of cross-spectrum matrix $\mathbf{R}(f_l)$ is

$$\mathbf{R}(f_l,t_q)=\mathbf{U}(f_l,t_q)\mathbf{\Sigma}(f_l,t_q)\mathbf{V}^{\mathrm{H}}(f_l,t_q)\,. \tag{3.9}$$

The MUSIC signal processing method is applied to each time segment. The MUSIC power of q-th time segment is defined as

$$P_{\mathrm{MUSIC}}(f_l,S_n,t_q)=\frac{1}{\sum_{i=p+1}^{M}\left|\mathbf{g}^{\mathrm{H}}(f_l,S_n)\cdot\mathbf{u}_i(f_l,t_q)\right|^2}\,, \tag{3.10}$$

where p is the dimension of the signal subspace. $\mathbf{u}_i(f_l,t_q)$ is the i-the column of the matrix $\mathbf{U}(f_l,t_q)$ is Eqn. (3.9). $\mathbf{g}(f_l,S_n)$ is steering vector.

Eqn. (3.10) shows that the MUSIC power is changing with respect to time. The MUSIC power image reveals the source location at time t_q.

3.2 SHM with Non-GUW Excitation

In this part, we present a case of SHM with non-GUW excitation over a pipe. The excitation frequency is in the audible frequency range, of which the wave propagation characteristic is less complicate than that of GUW. The case is presented to demonstrate that the locations of measurements play an important role for SHM of pipe structure.

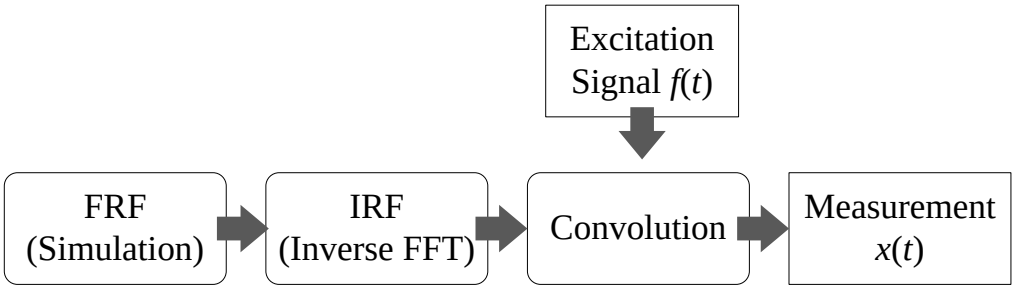

Figure 7. Data flow for obtaining the time response.

3.2.1 FE Simulation

Figure 7 shows the process to obtain the time response for simulation. First the frequency response function (FRF) is obtained from FE simulation. FRFs are converted to impulse response function (IRF) by inverse FFT. The measurement is the time response, which is obtained from convolution of excitation signal $f(t)$ and IRF.

An ANSI 1¼ inch schedule 40 pipe is the interested pipe model in both simulation and experiment. The outer diameter of the pipe 42.2 mm and the thickness is 3.55 mm. The pipe is made of stainless steel, of which the density is 7400 kg/m^3. Its Young's modulus is 201 GPa and Poisson's ratio is 0.285. The structural defect is hole with through wall thickness and 15 mm diameter. The 3-D FE model of this pipe is built in the commercial software ANSYS [40], as shown in Figure 8.

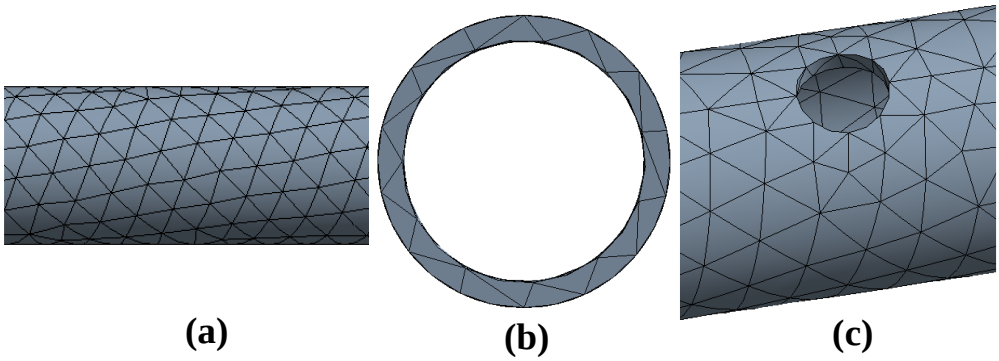

Figure 8. 3-D FE model of ANSI 1¼ inch schedule 40 pipe. (a) side view; (b) cross-section view; (c) meshes around the structural defect.

As shown in Figure 8, the 3-D linear solid tetrahedron element is adopted for this pipe model. Figure 8(a) shows part of the pipe wall in axial direction. Figure 8(b) shows the zoomed in cross-section view. Figure 8(c) shows the mesh around the structural defect.

The FRF is obtained from harmonic analysis by model supposition method [39]. The maximum frequency component of the FRF is set to 4 kHz. To obtain an accurate result, the maximum frequency for the modal analysis should be larger than 1.5 times of the maximum frequency of harmonic analysis. In this case, the maximum frequency for the modal analysis is chosen as 7 kHz, of which the corresponding wave length is 0.2184 m. The size of the element is chosen as 0.01 m, which is less than 1/20 wavelength.

3.2.2 Experimental Validation

The FRFs obtained from simulation is validated by an experiment. The photo of pipe modelled in the simulation is the shown in Figure 9.

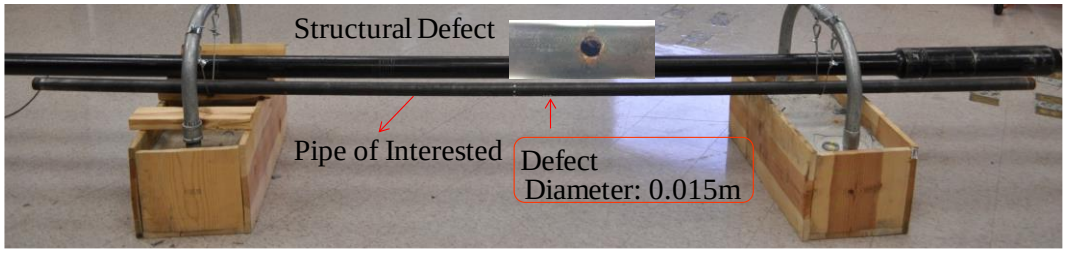

Figure 9. Photo of an ANSI 1¼ inch schedule 40 pipe with a circular shape structural defect.

As shown in Figure 9, the pipe with smaller diameter is the interested pipe. The pipe is suspended by two steel strings. Within the considered frequency range, the effect of these hanging strings is negligible. The boundary condition of the pipe is treated as free-free boundary condition. The structural defect is a hole, of which the diameter is 0.015 m. The size of the structure defect is the same as the one in the simulation.

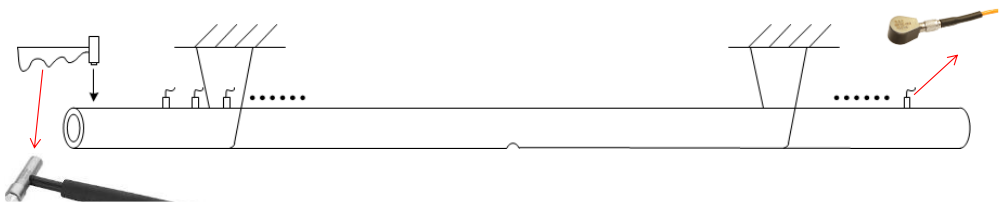

Figure 10. Experimental setup for FE model validation.

The experimental setup is illustrated in Figure 10. A Bruel & Kjaer (Model 8206-001) impact hammer generates the excitation signal by hitting one end of the pipe. The input force is perpendicular to the pipe as indicated by a black arrow in Figure 10. The excitation point is 0.026 m to one end of the pipe. A Bruel & Kjaer (Model 4571) one-direction accelerometer is used to scan the frequency response at different locations

along the pipe. The spatial sampling interval, which is distance between two adjacent measurement locations, is 0.1m. There are 30 measurements in total. The excitation signal from the impact hammer and the response signal from the accelerometer are processed by the Pulse sound and vibration analyser system (Model 3560B) from Bruel & Kjaer.

The comparison between the FRFs from simulation and experiment is shown in Figure 11.

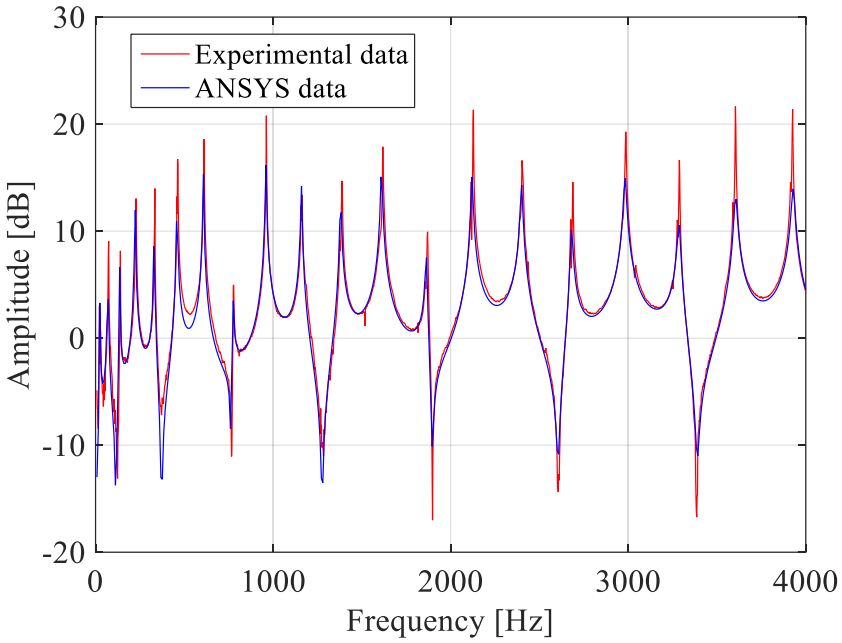

Figure 11. Comparison between FRFs obtained from experiment and simulation.

Figure 11 shows the comparison the FRF at the location 1.932 m. The blue line is the FRF obtained from the 3-D FE simulation. The red line the FRF obtained from experiment. The two FRFs match well in the frequency range up to 4 kHz, because they

have the same resonant frequencies and anti-resonant frequencies. At the resonant frequency the experiment data has higher peaks, which indicate that the structural damping coefficient of the pipe is lower than that in the FE simulation. This comparison proofs the current element type and mesh size is fine enough to simulate the behavior of the actual pipe when the excitation frequency is less than 4 kHz.

3.2.3 Simulation Results

Since the low frequency excitation is one-dimensional (1-D) flexural plane wave [41], the pipe is also abstract as a 1-D structure. The simulation setup is shown in Figure 12.

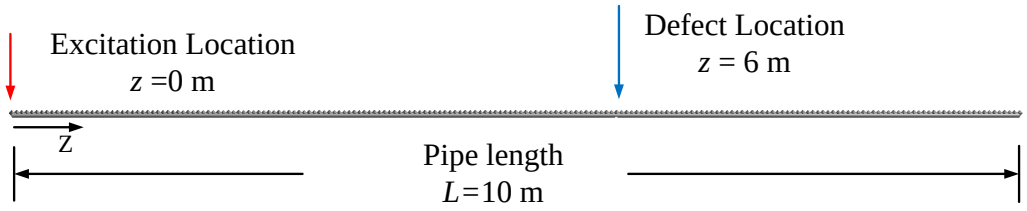

(a)

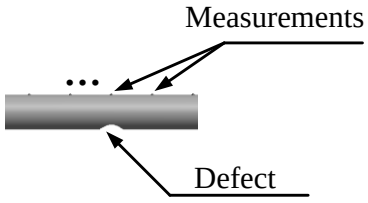

(b)

Figure 12. Simulation setup for SHM with non-GUW. (a) Locations of point force excitation and structural defect; (b) Zoomed in view nearby structural defect.

A 1-D flexural wave excitation of 2.5 kHz is generated by applying a point force perpendicular to the pipe axial direction at z = 0 m, as shown in Figure 12(a), indicated by the red arrow. The structural defect is a circular hole with a diameter of 0.015 m at z = 6 m, indicated by the blue arrow. The zoomed view of the structural defect is shown in Figure 12. The measurements (marked as the circular dots) were located on the surface of the pipe along the axial direction and the spatial sampling space was 0.05 m. The number of measurements linearly increases regarding the length of the pipe.

The excitation is five cycles 2.5 kHz sinusoidal wave turned by a Hanning window as shown in Figure 13.

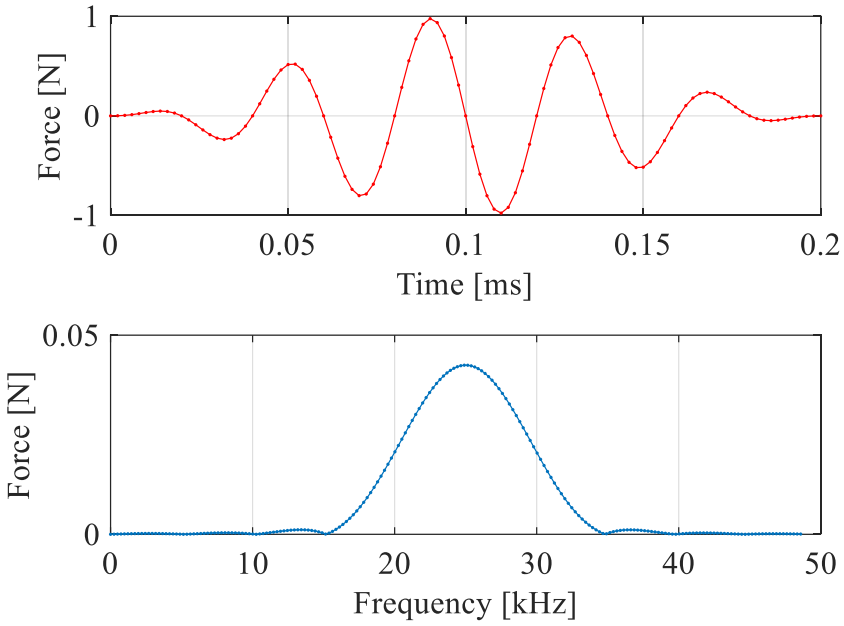

Figure 13. Excitation signal in time domain (top) and frequency domain (bottom).

Figure 13 shows the excitation in time domain and frequency domain. In time domain, the excitation is a burst signal turned by a Hanning window. Its duration is around 0.2 ms. The frequency spectrum of the excitation shows that the excitation frequency is centered at 2.5 kHz.

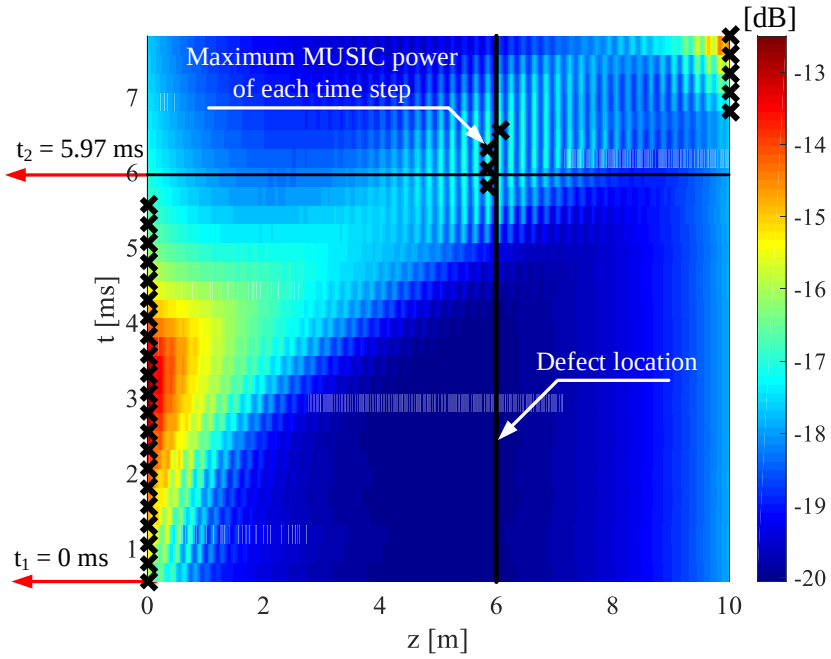

Figure 14. MUISIC power of pipe obtained with TF-MUSIC method.

Figure 14 shows the MUSIC power in dB scale. The MUSIC power is a function of the axial pipe location (*z*-axis) and the time (*t*-axis). The MUSIC power is obtained by using the TF-MUSIC method. For each time segment, indicating as each row of the image, there is a black "x" mark indicating the maximum MUSIC power for the current time segment. The black line indicates the actual location of the structural defect.

At the time of $t = t_2$, the excitation wave arrives at the structural defect location.

The structural defect becomes a passive source by reflecting the excitation at $t = t_2$. Therefor, the maximum MUSIC power happens at the structural defect at the time around t_2 Before t_2, the maximum MUSIC power locations indicate the excitation location. After t_2, the maximum MUSIC power locations indicate the boundary location.

This simulation case shows the importance of data acquisition system in SHM paradigm. In this case, the excitation wavelength is 40.2 cm, which is large compared to the diameter of the defect, which is 1.5 cm. However, with proper data acquisition system, the axial defect location is correctly visualized.

In this case, the transducer array is synthetically formed by all the measurements. This is a 1-D array along axial direction, since the excitation wave is 1-D wave. The disadvantage of this data acquisition system is that it requires a large number of measurement points. The number of the measurement increasing linearly regarding the length of the interested pipe, which is not favourable in real case. The data acquisition system will be improved in the next section when GUW is chosen as excitation.

3.3 SHM with GUW Excitation

The axisymmetric torsional GUW wave, *T*(0,1), is generated as excitation by the transducer array design presented in Section 2. In this section, we presented a creative data acquisition system design. We also justified that the number of measurements, so that it does not increase linearly regarding the length of pipe.

3.3.1 Dual Array Design

It has been demonstrated that a single transducer array identifies structural defects over plate structures [16]. However, MUSIC power is a monotonically increasing function of the distance between the scanning point the transducer array on small diameter pipes. This is caused by the fact that the axial location of the structural defect is dominantly determined by axially-propagating, planar GUW components. We justified that it is difficult to reveal defect locations using the MUSIC signal processing method with signal transducer array setting by a simple case. After that, we proposed a dual transducer array design and provided method to extract defect locations using the MUSIC power obtained on the new setting.

We first show the incompetence of the single array setting in the defect detection by a simplified beam model where only planar flexural waves are propagating through the beam. The circular beam is considered as a model to demonstrate the effect of single array and dual array over MUSIC power of the structure which has salient different curvatures in axial and circumferential directions. The radius of the beam is 21.1 mm and the beam has infinite lengths in both the positive and negative wave propagation directions. The beam is made of isotropic stainless steel with the density of 7400 kg/m^3 and the Young's modulus of 201 GPa. The structure damping coefficient is set to η = 0.001. A harmonic, point force excitation of frequency f_e = 10 kHz is applied at location z_e = 1.3 m. The excitation has a complex amplitude, F. The wave response in frequency domain at a measurement location of z_m is represented as

$$\mathrm{X}_m(f_e) = \frac{F}{4EIk(f_e)^3}\left(\mathrm{i}e^{jk(f_e)|z_m - z_e|} - e^{-k(f_e)|z_m - z_e|}\right), \tag{3.11}$$

where k = 33.804+0.085i is the wavenumber at the excitation frequency f_e = 10 kHz. The imagery part of k is determined by the structure damping coefficient. F is the amplitude of the excitation. I is the inertial of the cross-section area. j is the complex unit. $|\ |$ is the absolute value.

In this case, the steering vector is

$$\mathbf{g}(f_e, z_s) = \left[\mathrm{e}^{jk(f_e)|z_1 - z_s|} \quad \cdots \quad \mathrm{e}^{jk(f_e)|z_m - z_s|}\right], \tag{3.12}$$

where z_m is the measurement locations (m = 1, …, M), if the total number of measurement is M, where z_s represents the location of a scanning point.

In this analytical case, two transducer array deployment strategies are studied. In the first strategy, there is only one transducer array locates at z = [0, 0.01] m. The transducer spacing is less than half wave length, which satisfies the Nyquist sampling criteria. In the other transducer array deployment strategy, two transducer arrays are employed. One array is located at z = [1.00, 1.01] m. The other array is located at z = [1.99, 2.00] m. By applying Eqns. (3.11) and (3.12) into Eqn. (3.1) to Eqn. (3.4) with the signal subspace dimension, p = 1, we obtained the MUSIC power result for each measurement deployment strategy is shown in Figure 15.

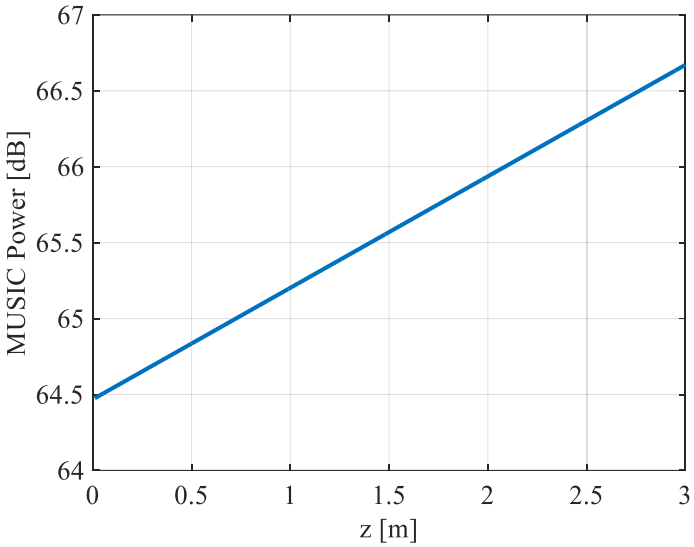

(a)

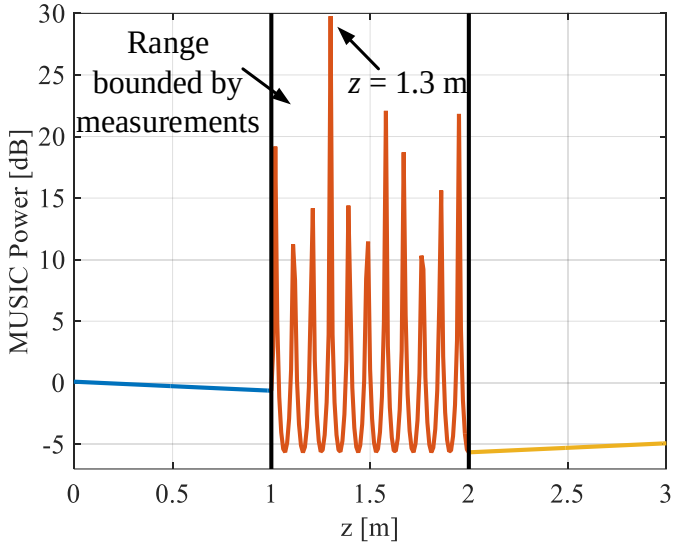

(b)

Figure 15. MUSIC power results. (a) Single array with 2 transducers at z_1 = 0 m and z_2 = 0.01 m and (b) Dual arrays with 4 transducers at z_1 = 1 m, z_2 = 1.01 m, z_3 = 1.99 m, and z_4 = 2 m. For the dual array, the first array has the transducers at the first two measurement locations (z_1 and z_2) and the second array has the transducers at the last two measurement locations (z_3 and z_4) [37].

As shown in Figure 15(a), when a single array with two measurements is placed at the left side of the point excitation, the MUSIC power monotonically increases when the scanning point moves away from the array, regardless the existence of the source. As a result, it is impossible to identify the excitation location. Figure 15(b) shows that in the region bounded by dual arrays, the excitation location is correctly detected by the maximum MUSIC power at z = 1.3 m. However, in the region which is not bounded by dual arrays, the MUSIC power remains monotonically increasing when the distance between scanning points and measurement array increases.

Therefore, it is concluded that the dual array design is required to identify the excitation location on a beam/pipe structure with MUSIC signal processing method. Additionally, only with region bounded by the dual arrays, the MUSIC power of scanning area represent its actual signal power.

The ultrasonic transducer array configuration proposed for small diameter pipe is shown in Figure 16. There are two transducer arrays. The SHM scanning area is bounded by both transducer arrays. Each transducer array is a ring-type array in the circumferential direction. The ring-type array has transducers evenly distributed around the circumferential direction of the pipe with the spacing satisfying the Nyquist sampling criterion.

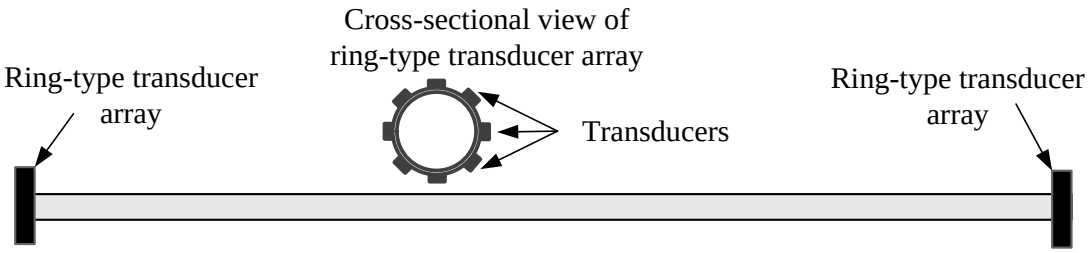

Figure 16. Ultrasonic transducer array design for MUSIC signal processing method on a pipe structure.

3.3.2 Simulation Setups

The ANSI 1½ inch schedule 5 pipe, of which GUW dispersion curves are considered in Section 2.1, was modelled in ANSYS. The FE mesh type is SOLID 185, which is a linear 3-D solid element. There are 144 elements in the circumferential direction and 3 elements in the thickness direction. In the axial direction, the size of each element is 3 mm. The FE model is shown in Figure 17.

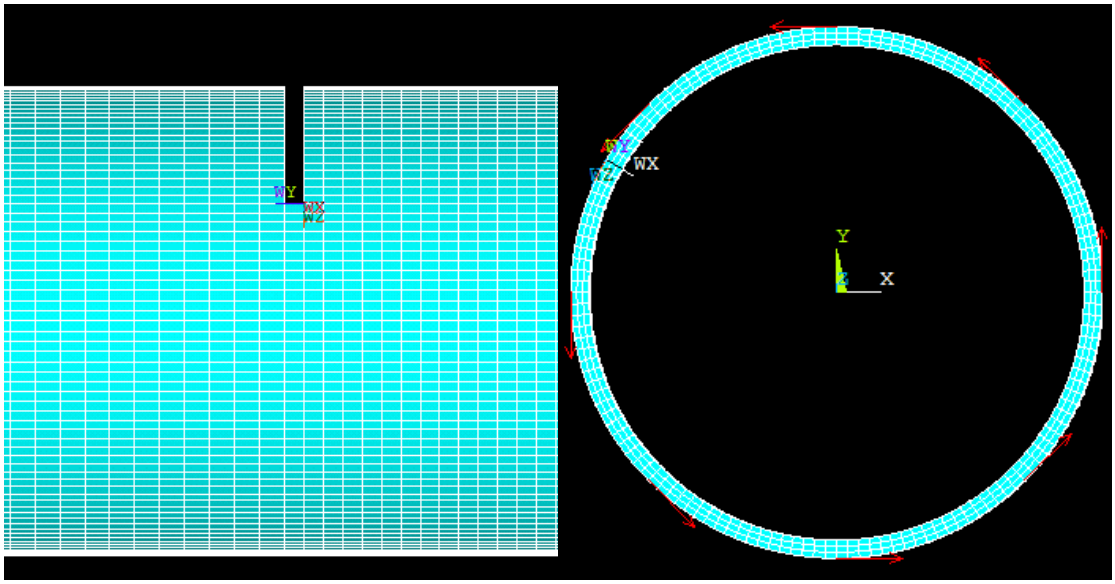

(a) **(b)**

Figure 17. FE model of ANSI 1½ inch schedule 5 pipe. (a) structural defect. (b) cross-section area and force.

Figure 17(a) shows the axial mesh and the structural defect. Figure 17(b) shows the mesh at the cross-section area and the force load. The *T*(0,1) GUW excitation is generated by applying the force with a same amplitude, 1 N, at 8 nodes which are distributed evenly in the circumferential direction at one end of the pipe indicated by red arrows in Figure 17(b). It simulates the excitation with 8 shear motion transducers.

Each force load is a burst sinusoid wave centered at frequency 30 kHz. Its amplitude is weighted by a Hanning window. The circumferential acceleration responses in time domain are obtained from all measurements in FE models. For this interested pipe, there are 8 measurement points at each end of pipe. In total, there are 16 measurement points. The time responses obtained from FE analyses are processed by MUSIC signal processing method introduced in Section 3.1.1.

Table 1. Five FE simulation cases.

Simulation Case #	**Structural Defect Size (d = 1.65 mm)**				**Transducer Array (L_1 = 1.828 m and L_2 =2 m)**	
	Circumferential Span	Off-Center Angle	Axial Span	Radial Depth	Location of Ring Array 1	Location of Ring Array 2
1	120°	0°	3 mm	d	0 m	L_1
2	90°	15°	3 mm	d	0 m	L_1
3	120°	0°	3 mm	$d/2$	0 m	L_1
4	120°	0°	3 mm	d	0.1 m	L_2-0.1 m
5	30°	0°	51 mm	d	0 m	L_1

Table 1 shows the configuration of five FE simulation cases. Simulation Case 1 is considered as a benchmark case. In this case, the structural defect has the circumferential span of 120°. The defect locates at the center of the unwrapped pipe in the circumferential direction. Therefore, its off-center angle is 0°, which means the angle between the center of the defect and the center of unwrapped pipe in circumferential direction is 0°. The axial span of the defect is 3 mm. The radial depth of the structural defect is d = 1.65 mm that is the same as the pipe wall thickness, indicating that this defect completely penetrates the pipe wall. Two transducer arrays are located at ends of the pipe to eliminate the boundary reflection. Each array has the ring-type array of 8 transducers. Simulation Case 2 is the same as the baseline case (i.e., Simulation Case 1) except that the structural defect in Case 2 has the circumferential span of 90° and is located at 15° off from the center of the unwrapped pipe. In Simulation Case 3, the

depth of the structural defect is reduced to 0.825 mm, which is half pipe wall thickness, which makes the defect-reflected signal weaker than that of Case 1. In Simulation Case 4, the pipe length is extended to 2 m and the transducer arrays are located at 10 cm away from the pipe ends, so that boundary reflections are presented in the measured data. In Simulation Case 5, the structural defect is an axial slot instead of circumferential slot.

3.3.3 Simulation Results

Figure 18 shows the pipe images obtained by applying the MUSIC signal processing method to the measurements. In Figure 18, the pipe is unwrapped regarding an axial cut to form a 2-D surface. The distance between each scanning points and a measurement is their Euclidean distance on the 2-D unwrapped pipe surface. Figure 18 shows the MUSIC powers in the entire scanning area for the benchmark case (i.e., Simulation Case 1 in Table 1). The red squares indicate the locations of physical transducers. Red "x" is maximum MUSIC power locations. The area enclosed by the red line is -0.05 dB region to the maximum MUSIC power. The area enclosed by black line indicated locations and dimensions of the defect. The areas, enclosed by the red lines (i.e., -0.05 dB lines) around the red "x" marks, can be interpreted as the detected structural defect areas.

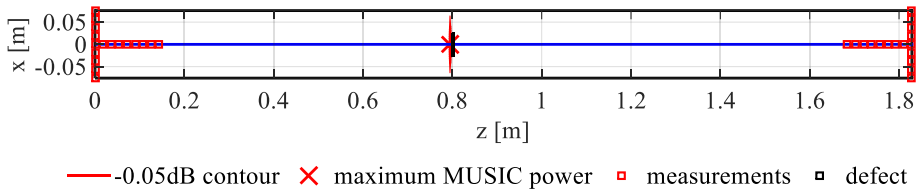

(a)

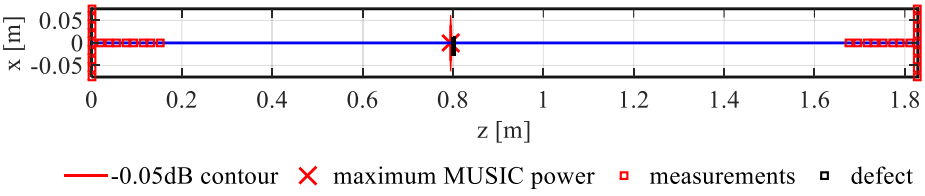

(b)

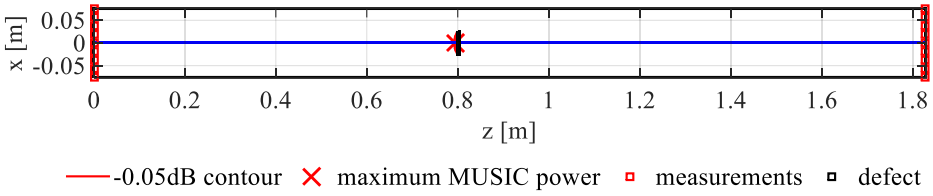

(c)

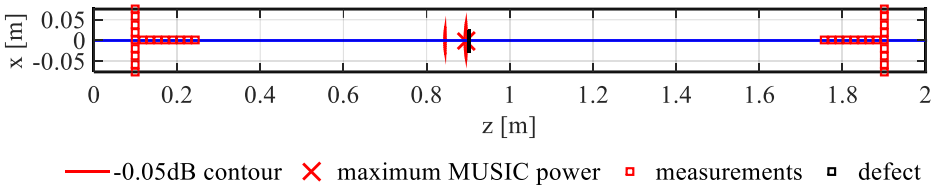

(d)

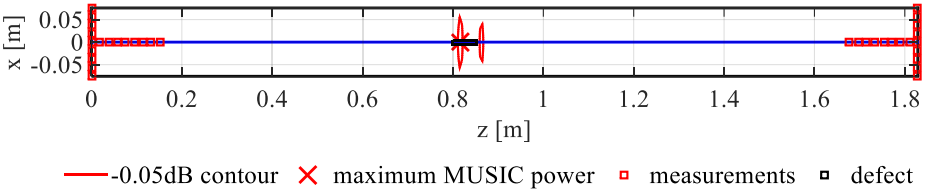

(e)

Figure 18. SHM result of ANSI 1½ inch schedule 5 pipe with dual transducer array setting and MUSIC signal processing method. (a) – (e) SHM result of simulation Case 1-5 in Table 1.

For all Simulation Cases in Figure 18, maximum MUSIC power locations (indicated by the red "x" marks) is the predicted defect location. The prediction error is defined as the distance between the predicted structural defect location and the center of the actual defect location. As shown in Figure 18, the prediction error has two components. One is the x-direction error, i.e., the circumferential error. The other is the axial direction error, i.e., the axial error. In Case 1,2,4,5, a linear transducer array is added in the axial direction.

For the benchmark case, shown in Figure 18 (a), the defect is located at the circumferential center of the unwrapped the pipe. The circumferential error is zero. The contour line indicates the shape of the structure defect. For Case 2, shown in Figure 18 (b), there is 15^{o} off-center angle between the center of the defect and center of the unwrapped pipe in the circumferential direction. In Case 2, the circumferential error is 15^{o}. The maximum MUSIC power still locates at center of the unwrapped in pipe in the circumferential direction, which means this method fails to predict the circumferential location of the defect. For Case 3, shown in Figure 18 (c), the location of the defect is the same as Case 2, but the depth of the structural defect is 0.825 mm, which is only half wall thickness. The defect-reflected GUW has smaller amplitude and the system has lower SNR. However, the axial defect location is still correctly detected.

For Case 4, shown in Figure 18 (d), when the transducer array is off the boundary of the pipe, the prediction error is not changed. However, there is an extra contour due to the boundary reflection. Similarly, there is an extra contour in Case 5, shown in Figure 18 (d), when the defect is a slot in axial directions.

All the cases have a constant 8 mm error. To address this problem, the dual excitation method is introduced. Note that there is a ring type transducer array at both ends of the pipe. Either one can be used as an excitation. In dual excitation method, the final MUSIC power result is generated by the summation of two parts. The first part is the MUSIC power of the unwrapped pipe obtained when the excitation is generated by the transducer array at the beginning of the pipe, $z = 0$ m. The second part is the MUSIC power obtained when the excitation is generated by the transducer array at the end of the pipe, $z = 1.8$ m. By adding these two parts together, we have the pipe image shown in Figure 19.

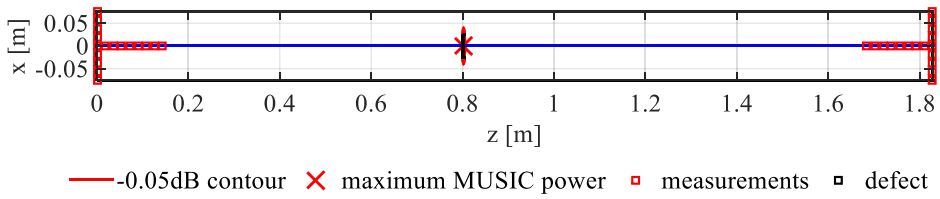

Figure 19. Pipe image for simulation Case 1 in Table I with dual excitation.

As shown in Figure 19, both the axial error is reduced to zero. Additionally, the contour shaper is aligned with the size of the defect. The structure defect is correctly visualized in the pipe image.

3.4 Conclusions

Two SHM paradigms are presented in this section. The data processing methods in both paradigms are based on MUSIC signal processing method, which is adopted

from that of plate structure. MUSIC method is adopted because it has high spatial resolutions in defecting structural defects.

In the first SHM paradigm, the pipe is abstracted as 1-D structure because the non-GUW excitation has 1-D wave propagation characteristics. The measurements are located along the axial direction of the pipe. The measured signals are processed by TF-MUSIC method. The axial location of the defect is correctly detected in a simulation case. However, there are too many measurements in this paradigm, which is not practical in real world.

In the second SHM paradigm, $T(0,1)$ GUW is adopted as the excitation to reduce the number of measurements. In this paradigm, the dual transducer array data acquisition system is proposed. MUSIC signal processing method is adopted to extract the defect information from the measurements. Five simulation cases are presented to validate this paradigm. When the defect is located at the center of the unwrapped pipe, the circumferential location of the defect is correctly detected. A constant axial error is observed in all cases. This error is removed by using the dual excitation method. Because of the computation cost for simulation, only the benchmark case is presented to validate the dual excitation method.

The advantage of using GUW as excitation is that the number of measurement can be significantly reduced. With dual array data acquisition system, the axial defect location over small diameter pipe structure can be correctly visualized with MUSIC signal processing method.

4. STRUCTURAL DEFECT IDENTIFICATION: AXIAL LOCATION AND CIRCUMFERENTIAL LOCATION

To detect the circumferential defect location mainly depends on analyzing differences of between measurements in the circumferential direction. However, when the axial dimension of the pipe, i.e., length, is much larger than the circumferential dimension of the pipe, i.e. diameter, measurement differences in the circumferential direction is very small. As a result, it is hard to obtained correct circumferential defect location.

A popular method to identify the circumferential defect of a pipe is the focusing method. This method is only applicable when the axial location of the defect is shown. Once the axial location of the defect is given, the transducer array is tuned to scanning a certain circumferential region at this specific axial location. When the defect presents, the transducer array will measure an enhanced defect-reflected wave. Therefore, the circumferential location of the defect can be identified. The disadvantage of this method is 1) angular profile of the pipe is required, so that the transducer array can be tuned to focus on a specific location, 2) the excitation frequency is range from 300 kHz to 500 kHz, which is not suitable for detecting the axial location of the defect at the same time.

In this section, two new methods are proposed to identify the circumferential and the axial locations of a defect simultaneously. In both proposed methods, no baseline data is needed and the excitation frequency is relatively low.

4.1 Geodesic Distance MUSIC (GD-MUSIC) Method

It is validated that MUSIC method can visualize the structural defect with a high spatial resolution. However, this method requires the information of the defect-reflected GUW propagation path to locate defects correctly. To describe the defect-reflected GUW propagation path accurately in the circumferential direction is the key to find the circumferential location of the defect. For small diameter pipes, the defect-reflected wave consists of multiple modes with different propagation characteristics. To our knowledge, there is no way to represent them analytically. In this method, we assume that defect-reflected GUW propagates along the geodesic path of the 3-D cylindrical surface of the pipe.

4.1.1 GD-MUSIC Method

When the defect-reflected GUW travels along a pipe, there are at least two paths in the circumferential direction, which are clockwise and count-clockwise. For example, if the scanning location locate is located at 1 in circumferential direction, as shown in Figure 20, there are at least two paths for the wave to propagate from location 1 to location 10 in circumferential direction. The first path is 1→12→11→10. And there is another path which is 1→2→3→4…→9→10. The circumferential distance of each path is different.

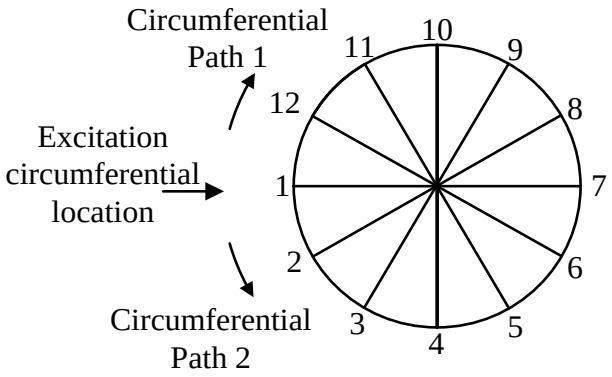

Figure 20. Multiple propagation paths of defect-reflected wave in circumferential direction.

In GD-MUSIC method, it is assumed that the defect-reflected wave propagates along the geodesic path in the circumferential direction. In other words, we assume the defect-reflected wave propagates along the shortest helix curve connecting two points, i.e., the geodesic path, on the 3D cylinder surface. The geodesic distance, denoted as r, between the scanning point and measurement is obtained from the following expression

$$r^2 = r_{circ.}^2 + r_z^2, \tag{4.1}$$

where r_z is the distance between the scanning point and the measurement in the axial direction and where $r_{circ.}$ is the geodesic distance between the scanning point and the measurement in the circumferential direction. The total distance between a scanning point and a measurement can be obtained by the Euler Equation.

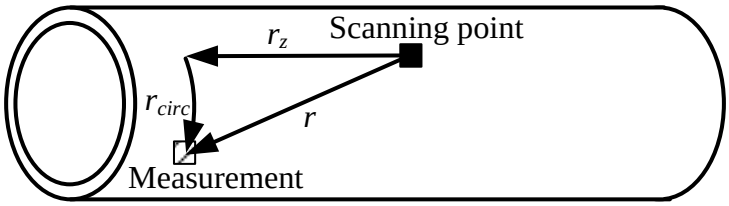

Figure 21. The geodesic distance of the defect-reflected wave is *r*. The axial distance between the measurement and scanning point is r_z and circumferential distance is r_{circ}.

Figure 21 illustrates how the geodesic distance is calculated by choosing the geodesic path as the defect-reflected GUW wave propagation path. The black square is a scanning point. The shadow square is a measurement point. The geodesic distance between the scanning point and the measurement is calculated from the axial distance between both points, r_z, and the geodesic circumferential distance between them, r_{circ}. This geodesic distance is used as the distance of the GUW propagating path for the steering vectors presented in Eqn. (3.5). The MUSIC power obtained from these steering vectors forms the pipe image for defect detection.

4.1.2 Simulation Setups and Results

The pipe model used in the simulation is an ANSI 4 inch schedule 5 pipe. Dimensions of this pipe type are, 0.1143m in diameter, 0.0021m in thickness and 1m in length. A FE model is built in commercial FEA software, ANSYS. The mesh type is solid95. This is a quadratic 3-D element. There are 20 nodes in each element. In this FE model, there are two elements in the thickness direction, and 120 elements in the circumferential direction. The element size in axial direction is 6 mm. The excitation is 5 cycles of sinusoid wave tuned by a Hanning Window. The centered excitation

frequency is 50 kHz. According to dispersion curves, the wavelength of $T(0,1)$ at 50 kHz is 61.58 mm. The distance between nodes is smaller than 1/20 of the wavelength, which is fine enough to capture wave propagation characteristics.

Figure 22 presents the FE model of the pipe. This model is built in ANSYS Mechanical. The axial extension of the defect is 6 mm, which is same as the element size in axial direction. The circumferential span of the defect is 60° as shown in Figure 22.

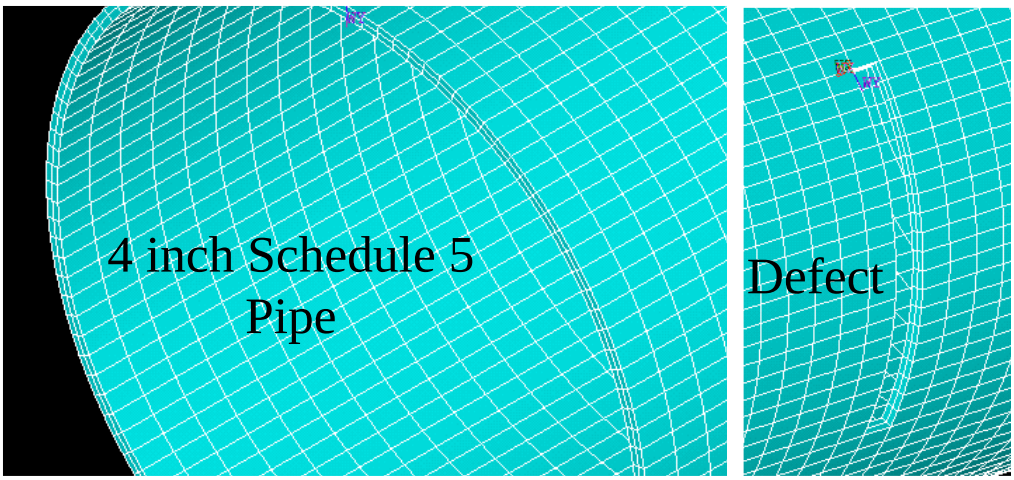

Figure 22. 3-D FE model of a defected ANSI 4 inch schedule 5 pipe. Left: cross-section view of the pipe. Right: structural defect.

The FE model with the free-free boundary condition is analysed with transient structural dynamics analysis in ANSYS Mechanical. Excitation forces are applied to 60 nodes, which are evenly distributed along the edge of the outer surface of the pipe. The direction of the force is θ-direction, when system coordinates are considered as cylindrical coordinate frames. The transient force is read into the system as a table, in

which the value of the force is listed with respect to time. The simulation result is shown in Figure 23.

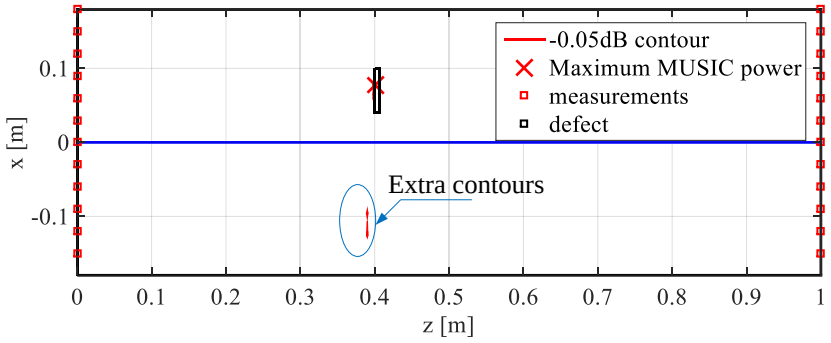

(a)

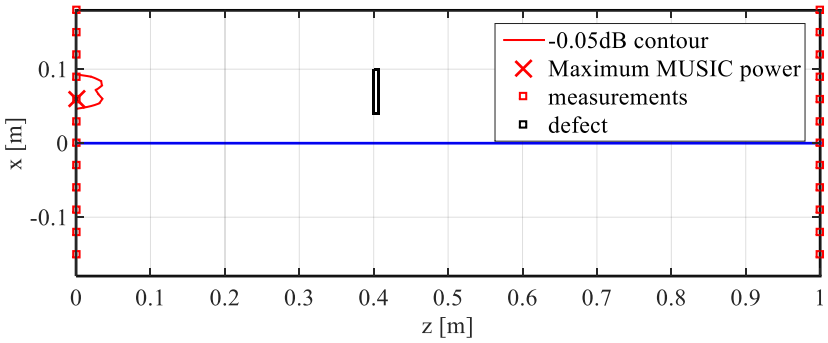

(b)

Figure 23. MUSIC power results when the different GUW propagation distances are used in steering vectors. (a) MUSIC power result when the distance *r* in steering vectors are calculated from geodesic paths; (b). MUSIC power result when the distance *r* in steering vectors are calculated from a non-geodesic paths.

In GD-MUSIC method, we calculate the GUW propagation path in 3-D surface, but we still present the MUSIC power result on a unwrapped pipe in 2-D surface for convenience. Note that the unwrapping does not affect the result Figure 23 shows the MUSIC power result when using different paths for calculating the GUW propagation

distance in steering vectors. The MUSIC power is shown in dB scale. As shown in Figure 23(a), when the distance r in steering vectors is calculated from the geodesic path along the 3-D cylindrical pipe surface, the MUSIC power image visualize the location of the defect correctly. The global maximum MUSIC power location, indicated by a red "x", is the predicted location of the defect. The difference between the predicted defect location and the center of the defect is defined as the analysis error. In this case, there is 3 mm analysis error in axial direction and 6^o analysis error in circumferential direction. Note that, though there are more than one -0.05 dB contours, which are supposed to indicate the shapes of the defects, only one contour corresponds to the location of the defect. Other contours indicate a headroom for improvement on current method.

A comparison result is shown in Figure 23(b). In this process, instead of choosing the geodesic path in the circumferential direction, r_{circ}, we choose the path ($2\pi R$- r_{circ}), where R is radius of the pipe. Because r_{circ} is the geodesic path between the measurements and the scanning point, $\left(2\pi R - r_{circ}\right) > r_{circ}$ always holds. As we can see, with the non-geodesic path, the location of the defect cannot be correctly identified.

4.1.3 Normalized 2-D Steering Vector

The GD-MUSIC method can be further improved using normalized 2-D steering vectors. The 2-D cylindrical wave is used to model the wave propagation in steering vectors. The steering vector presented is Eqn. (3.5) is reformed as

$$\mathbf{g}(f_l, S_n) = \left[\frac{1}{\sqrt{r_1(S_n)}} e^{jk(f_l)r_1(S_n)} \quad \cdots \quad \frac{1}{\sqrt{r_M(S_n)}} e^{jk(f_l)r_M(S_n)} \right]^T \tag{4.1}$$

where S_n is the location of n-th scanning point, where r_i is the geodesic distance between the defect and i-th measurement point, and where k is the wavenumber at frequency f_l.

When the scanning location is very close to a measurement, the distance r will be approaching zero. To avoid the situation, the steering vector is normalized.

$$\mathbf{g} = \frac{\mathbf{g}}{\|\mathbf{g}\|_2}, \tag{4.2}$$

where $\|.\|_2$ is 2-norm of a vector.

The GD-MUSIC with 2-D normalized steering vector is applied to the same pipe model. The GD-MUSIC result is shown in Figure 24.

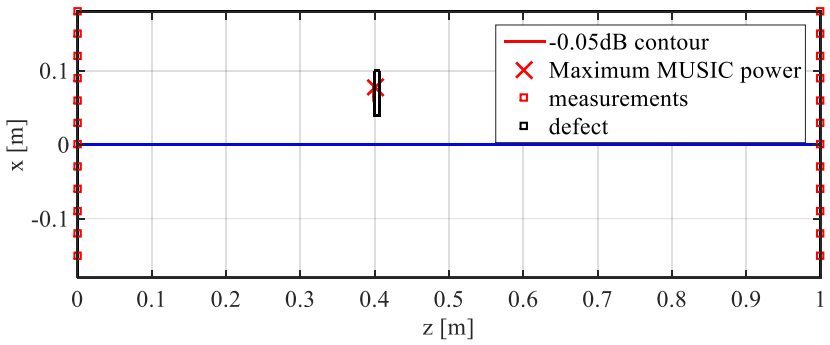

Figure 24. GD-MUSIC result with normalized 2-D steering vector.

As shown in Figure 24, with 2-D normalized steering vectors, the pipe image quality is improved by removing the extra contours compared to the pipe image generated by using 1-D steering vectors in Figure 23 (a). The predicted defect location, indicated by the red "x", remains the same as 1-D steering vector in Figure 23 (a).

Together with the simulation case presented in Figure 22, there are four simulation cases considered. The pipe model for each case is same, which is ANSI 4 inch schedule 5 stainless steel 304 pipe. The defect is different for each case. Details of the defects in each case are listed in Table 2.

Table 2. Four FE simulation cases.

Simulation Case No.	**Structural Defect Size (d = 0.083 inch)**		
	Circumferential Span	Axial Length	Radial Depth
1	60^o	6 mm	d
2	45^o	6 mm	d
3	60^o	6 mm	$d/2$
4	60^o	6 mm	d
	60^o	6 mm	d

Table 2 lists four simulation cases for an ANSI 4 inch schedule 5 pipe. Case 1 is treated as a benchmark case, of which the GD-MUSIC result is shown in Figure 24. The circumferential span of the defect is the same as the wavelength of $T(0,1)$ GUW at 50 kHz when traveling in this pipe model. In Case 2, the circumferential span of the

defect is reduced to 45^{o} (around 4.49 cm), which increases the difficulty of defect detection. In Case 3, the circumferential expansion of the defect is the same as Case 1, but the depth of the defect in *r*-direction is reduced from *d* to *d*/2, which means the defect does not penetrate the pipe wall. In Case 4, a multi-defect case is presented. Each defect has the same size but their circumferential locations are different.

The GD-MUSIC method is applied to the all the simulation cases listed in Table 2. The FE model for Case 2 to Case 4 has the same element type and mesh size as Case 1. The FEA processes for Case 2 to Case 4 are the transient structure analysis, which is the same as Case 1 as well.

The GD-MUSIC results of simulation Case 2 to 4 are shown in Figure 4.14(a) to (c).

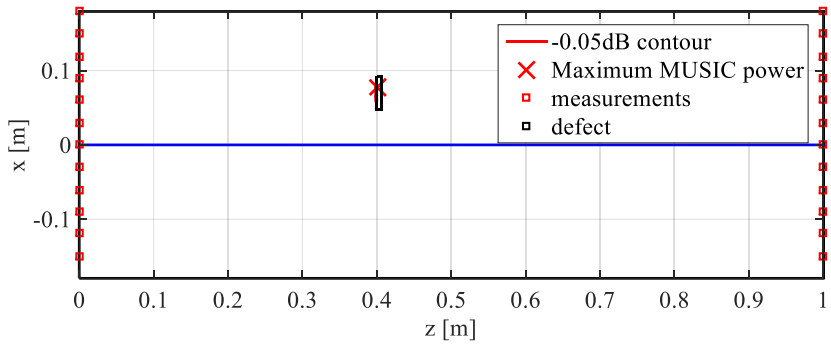

(a)

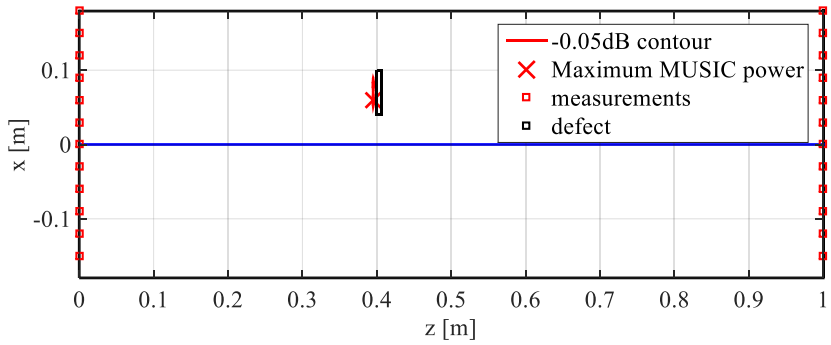

(b)

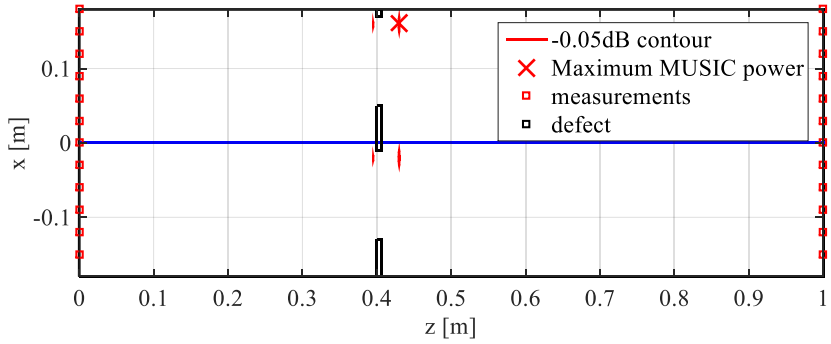

(c)

Figure 25. GD-MUSIC results for Case 2 to Case 4 with normalized 2-D steering vector. (a) GD-MUSIC result for Case 2; (b) GD-MUISC result for case 3; (c) GD-MUSIC result for case 4.

In Figure 25, the maximum MUSIC power is illustrated by the red "x". The defect region is indicated by -0.05 dB contour to the maximum MUSIC power. The red squares are measurement locations. The black lined box depicts the structural defect. The blue line is the center of the unwrapped pipe in the circumferential direction. For Case 2, of which the defect dimension in the circumferential direction is smaller than that of the benchmark case, Case 1, the defect location in both the circumferential direction and axial direction are correctly visualized with GD-MUSIC method as shown in Figure 25(a). The axial error, which is the difference between the maximum MUSIC power and the center of the defect in the axial direction, is 3 mm. The circumferential error, which is the difference between the maximum MUSIC power and the center of the defect in the circumferential direction is 8 mm (8^o).

For Case 3, the depth of the defect is a half of the pipe wall thickness, which means weaker defect-reflected GUW and lower SNR. The axial and circumferential location of the location are correctly visualized by the maximum MUSIC power. The axial error increases to 5.98 mm and the circumferential error increases to 10 mm (10^o). The pipe image from GD-MUSIC is shown in Figure 25(b). For Case 4, when there are multiple defects, the GD-MUSIC method fails to detect the two defects correctly, as shown in Figure 25(c).

In conclusion, with dual transducer array setting, GD-MUSIC method detects defect location in both the circumferential direction and the axial direction with high accuracy, when there is a single defect. However, GD-MUSIC method is not applicable for multiple defects, when the geodesic path assumption does not hold.

4.2 Predominant Component Voting MUSIC (PCV-MUSIC) Method

Given the fact that there is no general expression for the exact propagation path for a defect reflected GUW, a statistic method is proposed in this section. The defect locations, which are considered as the predominant components, will be correctly extract by the statistic process, i.e., voting.

4.2.1 PCV-MUSIC Method

In this method, the distance between the scanning point and the measurement are considered as the distance on the 2-D surface of the unwrapped pipe. Previously the pipe is unwrapped along a certain axial cut. However, the unwrapped method might introduce the error as shown in Figure 26.

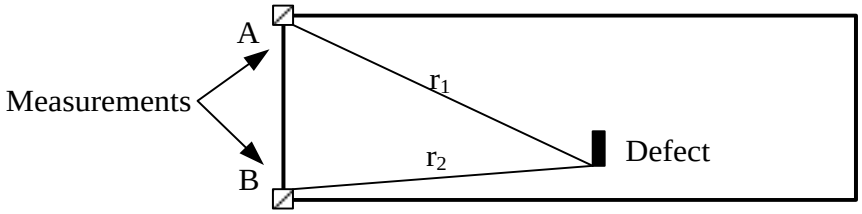

Figure 26. Illustration of the error introduced by unwrapping.

Figure 26 presents a case when the circumferential center of the defect is away from the circumferential center of the unwrapped pipe. The pipe is unwrapped along an axial cut started from the circumferential location of transducer A. The measurement from transducer A is repeatedly used at the location B, so that the continuity of the unrolled pipe is enforced. The location of the defect is indicated by the black block. The transducer A and B have the same measurement since they are the same transducer.

However, distances between a point on the defect and the transducer A, r_1, is different from that between the same point of the defect and the transducer B, r_2. This difference increases when the defect gets further away from the center of the unwrapped pipe, in the circumferential direction. The difference indicates that the MUSIC result for the unwrapped pipe is not accurate when the circumferential location of the defect is off-center.

Note that even the path between the defect and the measurements is considered in 3D cylindrical coordinate frame as presented in GD-MUSIC. The dilemma about the defect-reflected GUW propagation path still exists. The defect reflected wave can either travel along path r_1 or r_2 or both. Especially, since the defect-reflected GUW consists a non-axisymmetric component, the reflected torsional-flexural wave group $F(n,1)$ exists in the defect-reflected wave. The actual GUW propagation path cannot be determined without numerical simulation or experiment, which might not be practical in real cases.

The uncertainty in propagation path of the defect-reflected GUW prevents using the MUSIC signal processing method to get accurate results. To overcome this uncertainty, the PCV-MUSIC algorithm is introduced. In this method, the pipe is unwrapped along different axial cuts. When the pipe is unwrapped along different cuts, the circumferential location of the defect is different on the 2D unwrapped surface. Therefore, each unwrapped pipe is different from the others. Each unwrapped case is considered as a voter. The vote casted by each voter is the MUSIC power result of each case, obtained with MUSIC method. The votes are different from each other because the MUSIC power is computed based on the 2D unwrapped pipe surface. There are error in

each case, but they all contains the same dominant components which are defect locations. The voting result, which is obtained by combining votes from all voters, forms the final pipe image. Given the fact that the assumed defect-reflected GUW propagation path might not be exactly the same as the real case, the predominant components, i.e., defect locations, can be correctly extracted by voting. The PCV-MUSIC method diagram is illustrated in Figure 27.

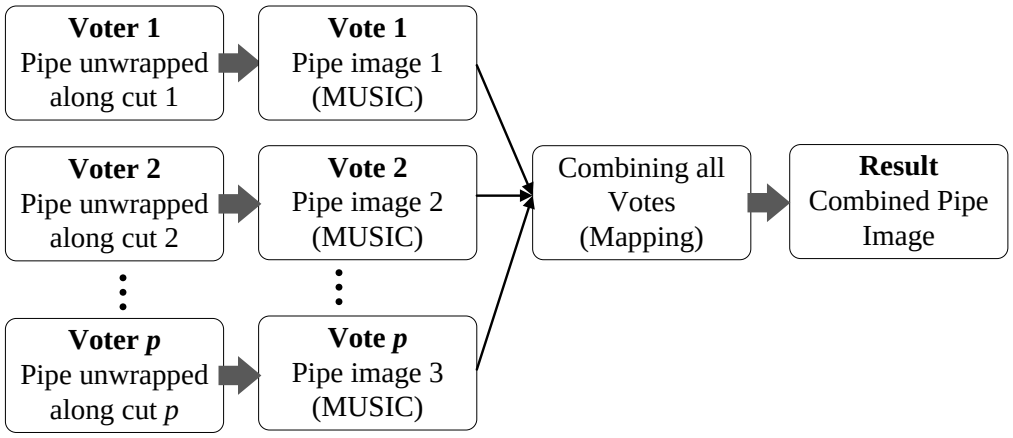

Figure 27. PCV-MUSIC method diagram.

As shown in Figure 27, there are p voters included in this poll. The voter is formed by unwrapping pipe with respect to different axial cuts. There is more than one way to decide axial cuts. To cut the pipe along the measurement locations in the circumferential direction is one way to decide the axial cuts. For example, if there are twelve transducers in the circumferential direction, there will be twelve voters when the pipe unwrapped with respect to an axial cut starting from each transducer circumferential location.

The location of the defect on each voter is different because the unwrapped location is different, as shown in Figure 28. There are 12 transducers at each end of the pipe. As a result, there are 12 voters generated by unwrapping the pipe along the 12 axial cuts. The axial direction of the unwrapped pipe is *z*-direction and the circumferential direction of the unwrapped pipe is *x*-direction.

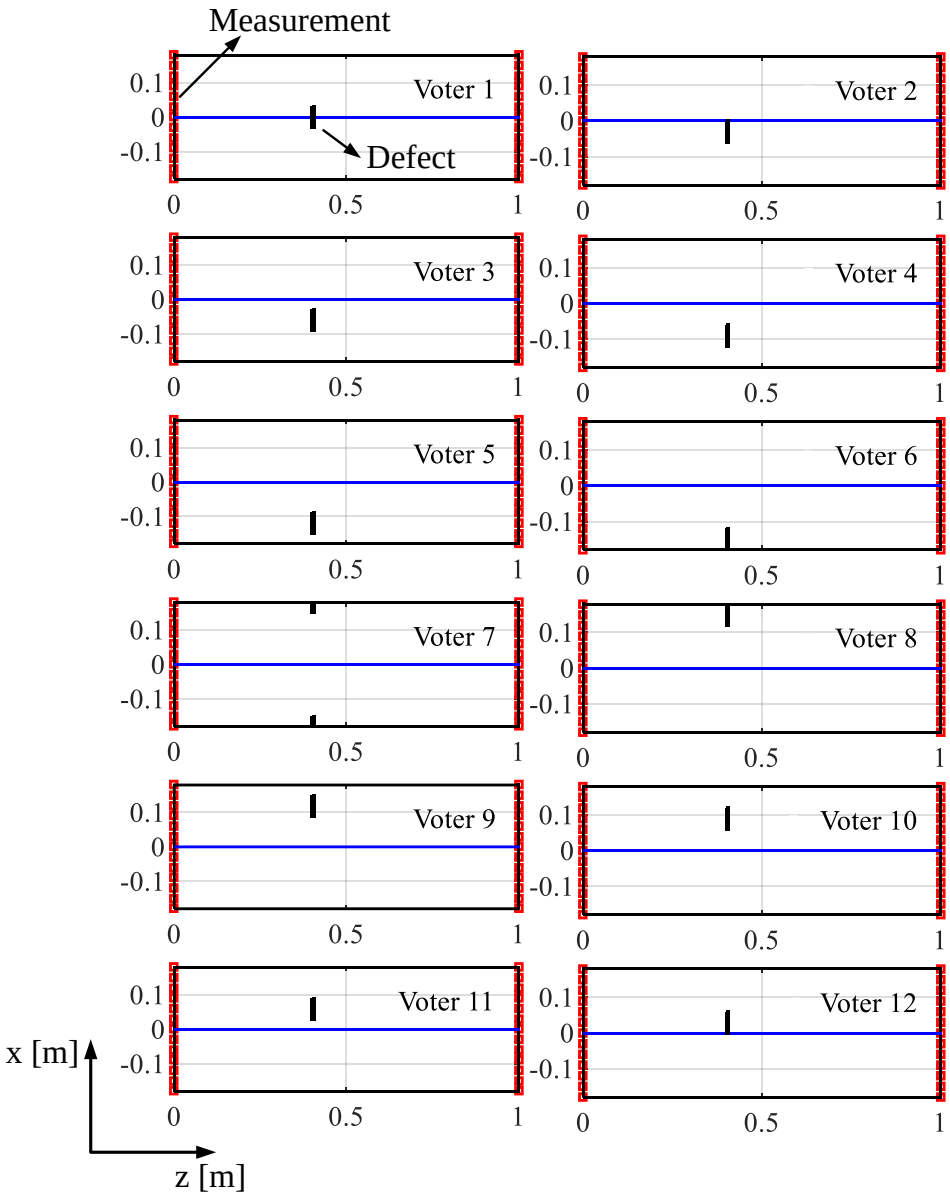

Figure 28. Twelve voters of 4 inch 1 m pipe fromed by unwrapping with respect to different circumferential locations. The defect circumferential location is different for each voter.

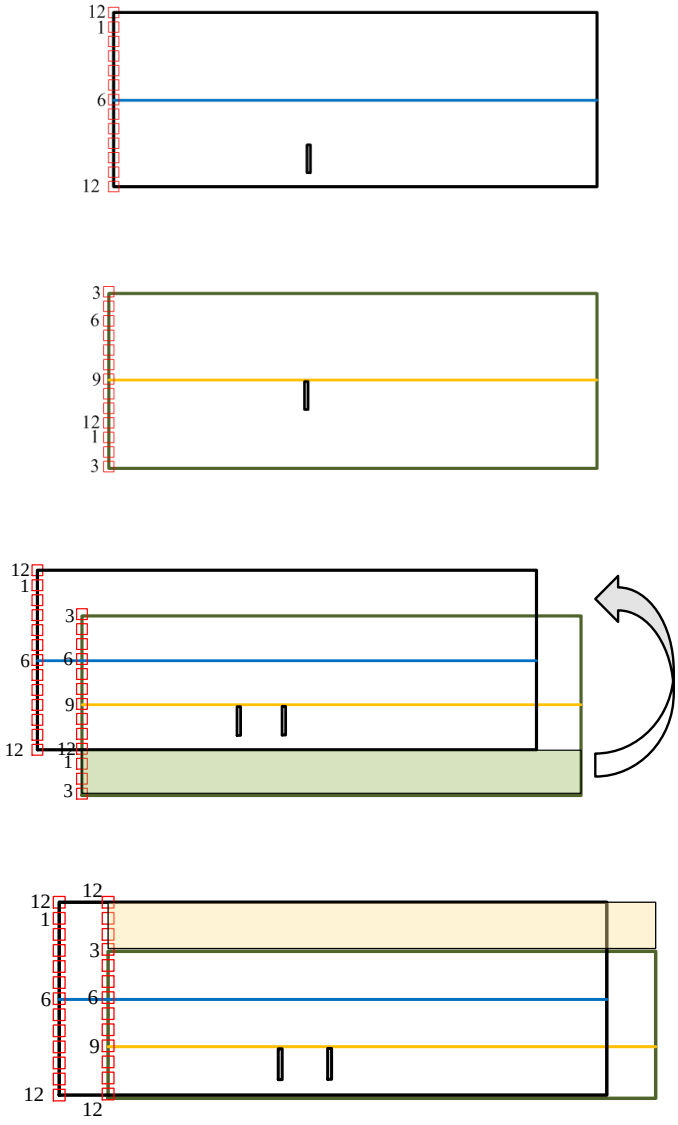

Figure 29. The mapping process. (a) the reference unwrapped pipe (i.e., reference vote). (b) a non-reference unwrapped pipe (i.e., a non-reference vote). (c)mapping the non-reference vote so that the defect location aligns up with reference vote. (d) mapped non-reference vote.

For each voter, MUSIC method is applied to 2-D surface of the unwrapped pipe. MUSIC power result, i.e., vote, is obtained from each voter. All votes are combined

together to form the final result. The combination process contains two parts. The first part is mapping. The second part is summation. In the mapping process, a vote is randomly chosen as a reference vote. All other votes are considered as non-reference votes. The non-reference votes are mapped so that the defect locations align up with the reference vote. The mapping process is illustrated in Figure 29.

The mapping process is illustrated without using the actual vote casted from each voter because the MUSIC power result affects the mapping result not mapping process. Therefore, the MUSIC power for reference vote and non-reference vote are not presented in Figure 29. Instead, Figure 29 shows the geometry settings of votes, which include the location of the defect, center of the unwrapped pipe and transducer positions. Without loss of generality, the reference vote is chosen as the MUSIC result of a pipe unwrapped along a axial cut starting at measurement location 12. The defect location of the unwrapped pipe is shown in Figure 29(a). The center of the reference voter is a blue solid line. The defect is indicated with a rectangular enclosed by black lines as boundaries. Similarly, Figure 29(b) shows the geometry of a non-reference vote, of which the pipe is unwrapped along an axial cut starting from measurement location 3. The defect location of this non-reference vote is shown on Figure 29(b). Figure 29(b) is mapped to the referee vote, which is unwrapped along measurement location 12, by shifting the bottom part (indicated in Figure 29 (c) as a green block) to the top (indicated in Figure 29(d) as a yellow block).

After mapping, the reference vote and non-reference vote are combined by summation. The final MUSIC power of the reference case, shown in Figure 29(a), is the

summation of all mapped non-reference votes.

4.2.2 Simulation Setups and Results

ANSI 4 inch schedule 5 pipes are modelled in this simulation. The outer diameter of the pipe is 4.5 inch and thickness of the pipe 0.083 inch. The length of the pipe is chosen as 1 m to reduce the computation cost. The element type is quad element 3-D solid element. There are 20 nodes in each 3-D element. There are two elements in the thickness direction. There are 120 elements in the circumferential direction. The element size in the axial direction is 6 mm. The excitation is 5 cycles of 50 kHz sinusoid wave tuned by a Hanning Window. The cantered excitation frequency is 50 kHz.

The finite element model with the free-free boundary condition is analysed with transient structural dynamics analyses in ANSYS Mechanical. The same excitation forces are applied to 60 nodes, which are evenly distributed along the edge of the outer surface of the pipe. The direction of the force is in the θ direction, when system coordinates are considered as in the cylindrical frame. The force is read into the system as a table, in which the value of the force is represented as a function of time.

There are four cases considered in this simulation. The pipe model for each case is the same. But, for each case, the defect is different. The detail of the defect in each case is listed in Table 2.

The simulation result of PCV-MUSIC method for Case 1 (the benchmark case), is shown in Figure 30.

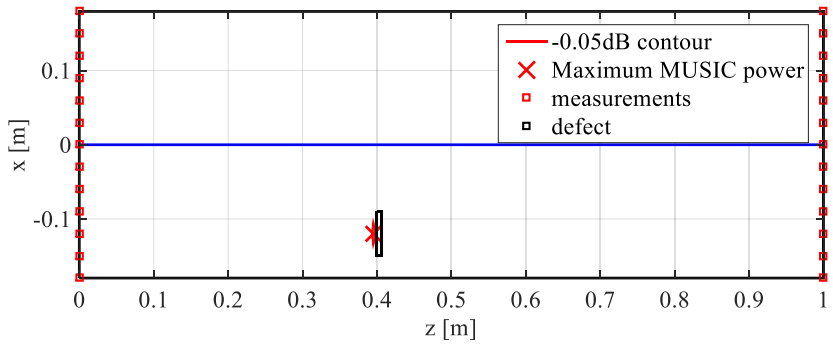

Figure 30. PCV-MUSIC result of Case 1: 4 inch schedule 5 pipe with the defect of 60º circumferential span (0.060m).

Figure 30 shows the pipe image generated by PCV-MUSIC algorithm. The measurements are located at both ends of the pipe indicated by red squares. The blue line is the center of the unwrapped pipe in the circumferential direction. The defect location is indicted by a rectangular area enclosed by black lines. In this case, the defect location is 120º off the center line of the unwrapped pipe. The maximum MUSIC power indicated by the red "x" is the location of the predicted defect. The distance between the prediction defect and the center of actual defect is the analysis error. The analysis error consists of two parts, circumferential error and axial error. In this case, the circumferential error is zero and the axial error is 8 mm.

Figure 31 shows the error analysis of MUSIC power results and PCV-MUSIC power results for all the voters.

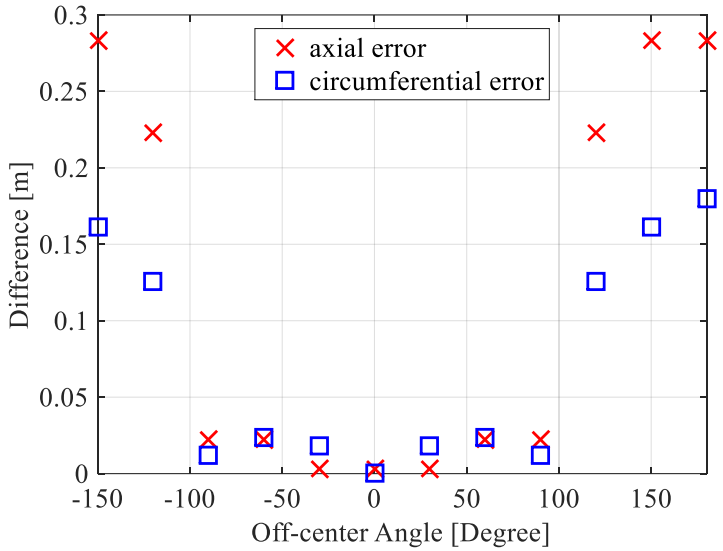

(a)

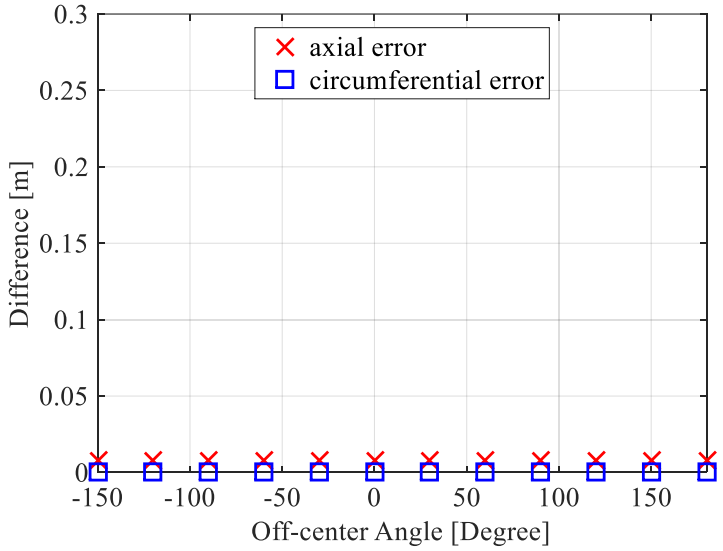

(b)

Figure 31. Error analysis of unwrapped pipes in both axial direction and circumferential direction. (a) Error analysis of MUSIC power results of unwrapped pipes; (b) Error Analysis of PCV-MUSIC results of unwrapped pipes.

In Figure 31(a) error changes when pipe is unwrapped with respected to different axial cuts. The off-center angle indicates the angle difference between the center of the defect and the center of the unwrapped pipe in circumferential direction. When the defect is at the center of pipe in circumferential direction, both the circumferential and the axial errors reach their minimum values. However, the error increases when the location of the defect leaves the center of the unwrapped pipe in axial direction. When the defect location is far from the center of the pipe, both the circumferential and the axial errors reach their maximum values. In Figure 31(b), the error of PCV-MUSIC method doesn't change with respect to different unwrapping methods. The circumferential error is zero and the axial error is a constant, which is 8 mm. The maximum error reduction in axial direction is reduced from 0.238 m to 0.008 m. The maximum error reduction in the circumferential direction is reduced from 0.162 m to 0 m.

The robustness of PCV-MUSIC method is validated with different simulation cases. The error of PCV-MUSIC method does not change with respect to reference vote. Therefore, without loss of generality, the reference vote is the one with the defect 120^{o} off the center of the unwrapped pipe.

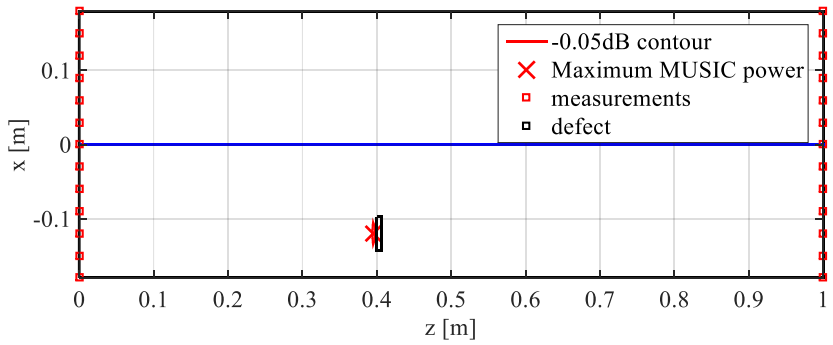

Figure 32. PCV-MUSIC result of Case 2: 4 inch schedule 5 pipe with defect of 45º circumferential span (0.044m).

In Figure 32, the circumferential span of the defect is reduced from 60º to 45º. The defect size is 72% of the wavelength of the cantered excitation frequency, 50 kHz. As we mentioned, the defect location is also 120º off the center. The error between the maximum MUSIC power and the center of the defect is same as Case 1. The axial difference is 8 mm and the circumferential differences is zero.

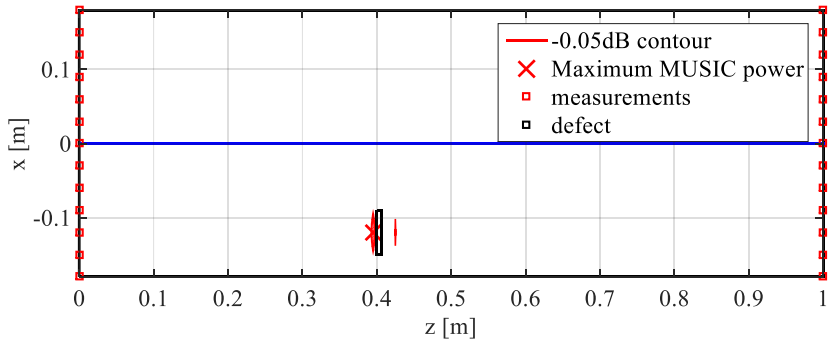

Figure 33. PCV-MUSIC result of Case 3: ANSI 4 inch schedule 5 pipe with defect of 60º span in the circumferential direction. The defect depth is half-wall thick.

In Figure 33, the circumferential span of the defect is the same as Case 1. But the depth of the defect is half-wall instead of through wall. The reduction of the defect depth reduces the amplitude of the defect-reflected wave, which, in turn, reduced the SNR. As a result, there is an another contour close to the location of the defect. The error between the maximum MUSIC power and the center of the defect is the same as those of previous cases. There is no error in the circumferential direction and 8 mm error in the axial direction.

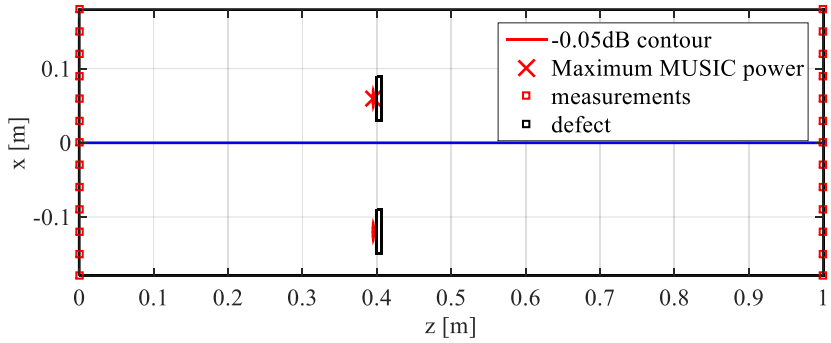

Figure 34. PCV-MUSIC result of Case 4: ANSI 4 inch schedule 5 pipe with multiple defects.

In Figure 34, there are two defects on the pipe of interest. Each of them has a 60^{o} circumferential span, which is that same as Case 1. The aim here is to detect the location of all the defects. As shown in Figure 34, the location of both defects are identified by the -0.05 dB contour. The maximum MUSIC power appears at the location of one of the defects. Moreover, the error between the maximum MUSIC power location and the location the defect which are close to each other, is same as previous cases. There is no circumferential error and the axial error is 8 mm.

The poll for each case shows that there is a local maximum MUSIC power at the location of defect. Despite noise in each figure, the final result of the vote correctly chooses the predominant component, which is the location of the defect, in both the circumferential direction and the axial direction. As shown in the error analysis, the error from the voted result is reduced by 97% compared to that of each vote from a single voter.

4.2.3 Robustness Analyses

In this section, the robustness of the PCV-MUSIC method is investigated. The aim is to find the applicable range for this signal processing method with the given 50 kHz excitation frequency.

Figure 35 shows the performance of PCV-MUSIC method, when the defect size decreases. In Figure 35(a), the defect size is half of excitation wave length. In Figure 35(b), the defect size is quarter of excitation wave length. When the size of defect decreases, energy of defect-reflected GUW also decreases. In other words, small defect corresponds to weaker passive source. As a result, SNR decreases and the other contours appear where there are no defects. However, the analysis error between the maximum MUSIC power location and the actual defect location remains the same, which is 0 mm in the circumferential direction and 8 mm in the axial direction.

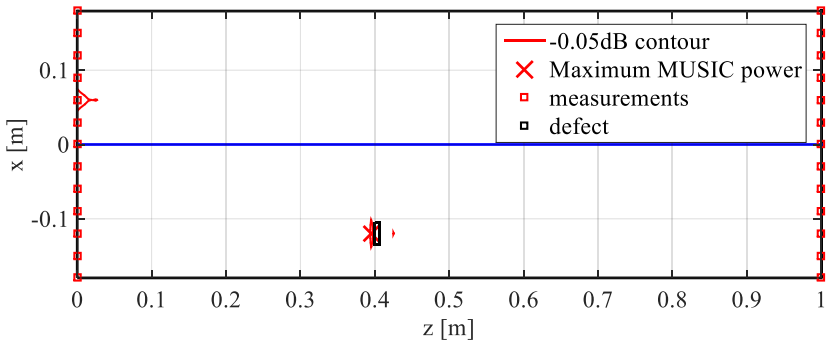

(a)

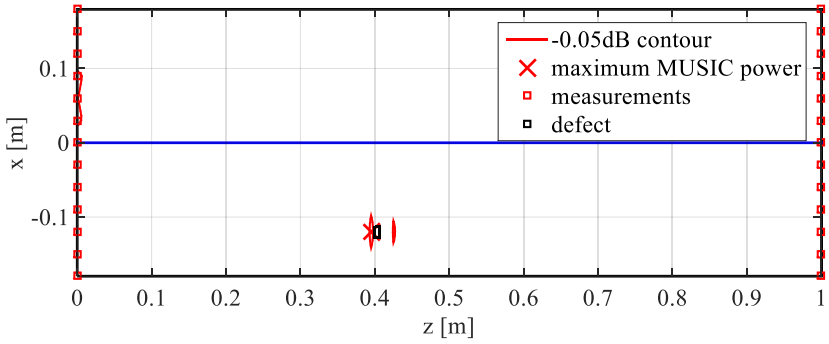

(b)

Figure 35. PCV-MUSIC results for different defect sizes. (a) the defect size is 30º, which is half excitation wave length. (b) the defect size is 15º, which is quarter excitation wave length.

Figure 36 shows the PCV-MUSIC result for a longer pipe, of which the length is 1.8 m. For a longer pipe, ratio of the circumferential dimension to the axial dimension decreases, which makes it harder to find the defect in the circumferential location. However, as shown in Figure 36, PCV-MUSIC method correctly predicts defect location. The analysis error in both circumferential direction is zero and axial direction is 8 mm, which is the same as previous cases.

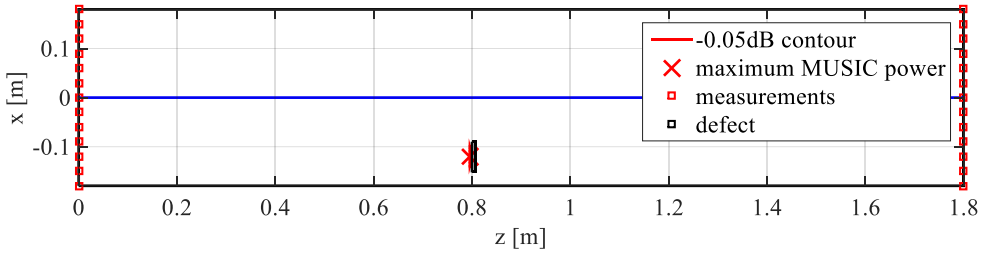

Figure 36. PCV-MUSIC results of a 1.8 m pipe.

4.3 Conclusions

To detect the circumferential locations of defects is much more difficult than to detect the axial locations of defects, because of the uncertainty of the defect-reflected GUW wave propagation path in circumferential direction. To detect the circumferential defect locations, two novel data processing methods are presented in this section. The first one is GD-MUSIC method. In this method, the defect-reflected wave is assumed to propagate along the geodesic path embedded in the 3-D cylindrical pipe surface. This method successfully detects defect location in both axial direction and circumferential direction simultaneously with a relative low frequency. However, this method is not suitable for multiple defect cases, of which the geodesic assumption does not hold. The other method is PCV-MUSIC method. In this method, the defect-reflected GUW is assumed to propagated along the Euclidean path on a 2-D surface formed by the unwrapped pipe. When the pipe is unwrapped with different axial cuts, the MUSIC result are different. Each unwrapped case is treated as a voter and its MUSIC power

result is referred as its vote. The error of this assumption is eliminated by combining votes from all voters together. The actual defect location, as the predominant component, is voted by all votes. The simulation results show that PCV-MUSIC method can visualized multiple defects correctly.

5. RECOMMENDED SCHEMA FOR EXPERIMENTAL VALIDATION

This section presents a recommended schema for experimental validation of proposed SHM paradigms. The schema consists two parts. One part is designing the device to generate the desired excitation. The other part is designing experimental setup and procedure. The pipe model of interest is an ANSI 1½ inch schedule 5 pipe with the length of 2 ft. The pipe is made of stainless steel 304. The experimental schema is suitable for all straight pipe of different materials and not limited to this specific pipe.

5.1 Transducer Gripper Design

The pipe of interest is an ANSI 1½ inch schedule 5 pipe with the length of 2 ft. The pipe is made of stainless steel 304. The Piezoelectric (PZT) transducers are used as both excitation and measurements in this experiment, considering the fact that PZT is one of the most common devices for GUW generation and measurement [42][43]. Dimensions of an ultrasonic transducer is decided based on dimensions of the pipe and the wavelength of the excitation GUW. The distance between two adjacent transducers should be less than half excitation wavelength to satisfy Nyquist sampling frequency. For a small diameter pipe, the ultrasonic transducer in a transducer array must be small enough so that there are sufficient measurements in the array for a given excitation GUW. The transducer also needs to provide enough excitation so that the defect-reflected GUW is detectable for the same type of transducer.

Figure 37 shows a photo of the transducer recommended for this experiment. To be compatible with 1½ inch pipe, the dimension of PZT transducers are customized as

7 mm width by 7 mm length by 5 mm thickness. The polarized surfaces are top and bottom surface as shown in Figure 37. The top surface is connected with a black lead by soldering, as shown in Figure 37. The electrode patterns for the bottom surface is side tap, and the red lead is soldered to the side tab of the bottom surface. The blue dot on the side surface indicates the displacement direction when the transducer is polarized. In this experiment, all transducers are made of the same APC 850 material, of which material properties are listed in Table 3.

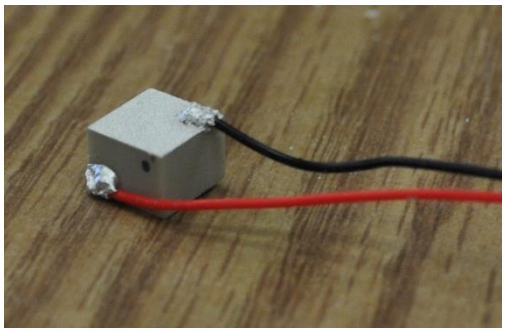

Figure 37. Photo of the piezoelectric transducer with soldered leads.

Table 3. Material properties of APC 850.

Piezoelectric Charge Constant (10^{-12} C/N or 10^{-12} m/V)			Piezoelectric Voltage Constant (10^{-3} Vm/N or 10^{-3} m^2/C)		
d_{33}	$-d_{31}$	d_{15}	g_{33}	$-g_{31}$	g_{15}
400	175	590	24.8	12.4	36.0
Electromechanical Coupling Factor				Young's Modulus (10^{10} N/m^2)	
k_p	k_{33}	k_{31}	k_{15}	Y^E_{11}	Y^E_{33}
0.63	0.72	0.36	0.68	6.3	5.4

To generate axisymmetric excitation, transducers are evenly placed in circumferential direction around the outer surface of the pipe, as shown in Figure 38. The lower bound of the measurement number is decided by Nyquist sampling criterion. On the 3D cylindrical surface, the geodesic distance between two adjacent transducers is smaller than half wave length of the excitation GUW. When an excitation voltage is applied, these transducers generate same shear motions and in turn generate axisymmetric torsional excitation waves.

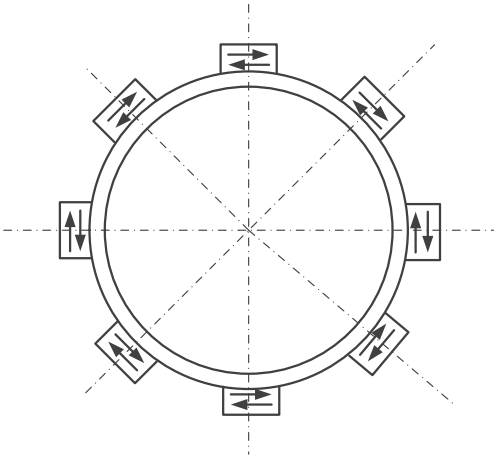

Figure 38. Cross-section view of the transducer array design. Arrows show directions of displacements when voltage is applied.

In Figure 38, there are eight transducers in the transducer array. This design is for the 1½ inch stainless steel 304 pipe and when the excitation is at 30 kHz. The number of the transducers varies when the outer diameter of the pipe changes or when the excitation frequency changes [44].

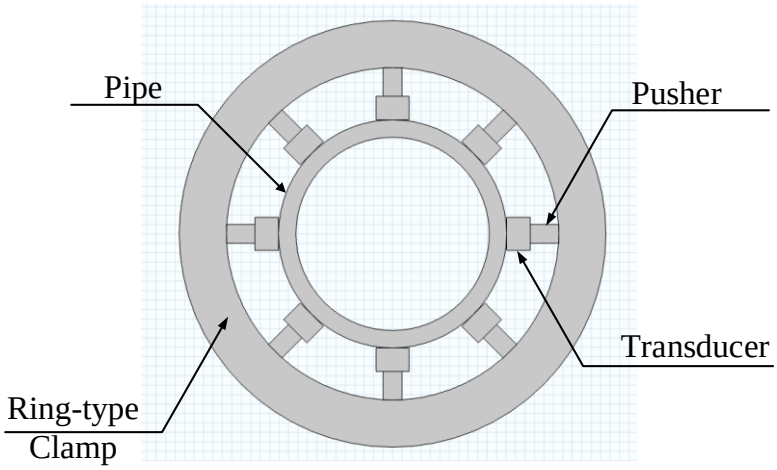

Figure 39. Cross section view of transducer gripper holding transducers against the outer surface of the pipe.

A transducer gripper is designed to place the transducers at desired locations and hold the transducers against the outer surface of the pipe. With this transducer gripper, the contacts between transducers and the pipe are mechanical. No bonding material is required between transducers and the pipe, so that the excitation and measurement location is changeable without re-apply the bounding material. Figure 39 shows the design of the transducer gripper in 2-D view. This transducer gripper consists of two parts. One is the ring-type clamp, which will be held by the robot arm. The thickness of this ring-type clamp is 10 mm. The other part is transducer pushers which push transducers to the pipe surface. Dimensions of each transducer pusher are 6 mm in height and 4 mm in width. The width of the pusher is less than that of the top surface of the transducer, so that contact surface between the pusher and the top surface of the transducer will not be effected by the soldering point of the lead.

The transducer array held by the transducer gripper is considered as a whole

system, which serves as both the excitation and the measurement system. A 2-D finite element is built for this system with COMSOL [45]. This simulation aims to prove that, with this design, the generated excitation has enough power so that so that the defect reflected wave is detectable by the same system.

Before the validation of the transducer gripper, a 2-D torsional spring is designed to compensate the missing torsional rotation inertia for this 2-D model. This process is shown in Figure 40 and Figure 41.

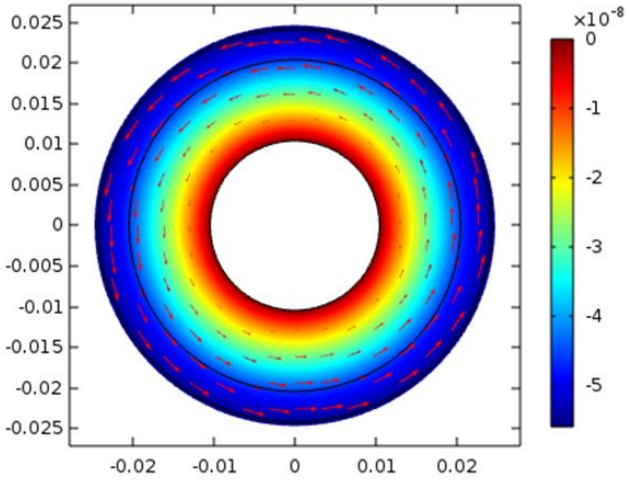

Figure 40. 2-D ANSI 1½ inch schedule 5 pipe model with torsional spring attached on the inner surface of the pipe.

Figure 40 is the cross-section view of the pipe attached with a torsional spring. When the thickness of the torsional spring is fixed, Young's module of this torsional spring is optimized so that the circumfenrtial deformation of the 2-D model is the same as that of the 3-D pipe model when same load is applied. Figure 41 shows the displacement of the 3-D model of the pipe. The red arrows indicate the direction and

amplitude of the displacement. The pipe has a fixed end colored in red at $z = 0$ m, where the displacement is zero. The torsional torque is applied at the free end colored in blue at $z = 1.8$ m, where the displacment is maximum.

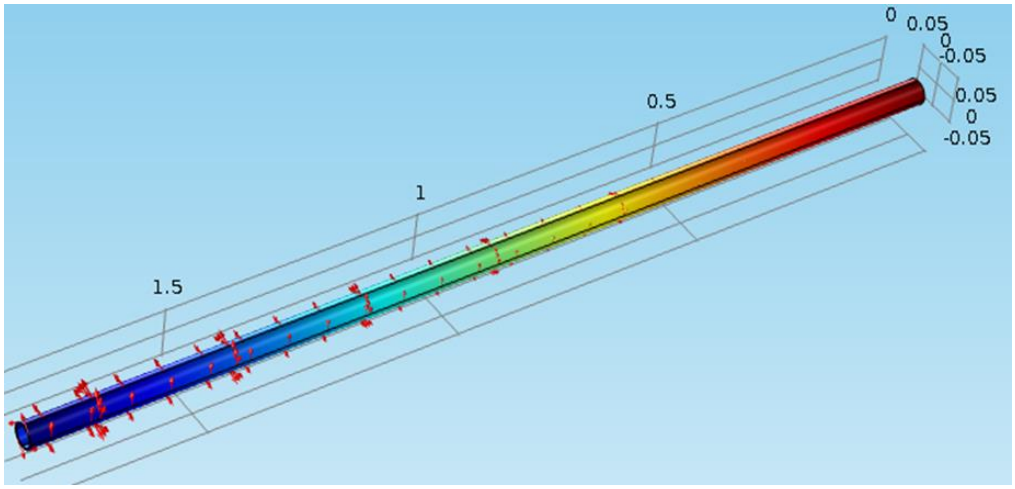

Figure 41. 3-D ANSI 1½ inch schedule 5 pipe model with the length of 1.8 m.

In Figure 41, one end of the 3-D pipe is fixed and the other end is free. The unit torsional torque is applied to the free end. The same torque is applied to the 2-D pipe model with the torsional spring. The value of Young's module of the torsional spring is adjusted, so that the 2-D model has the same displacement as the 3-D model. As a result, the 2-D model has the same torsional inertial and stiffness as the 3-D pipe model. This torsional spring will be added to the 2-D model for the transducer gripper validation.

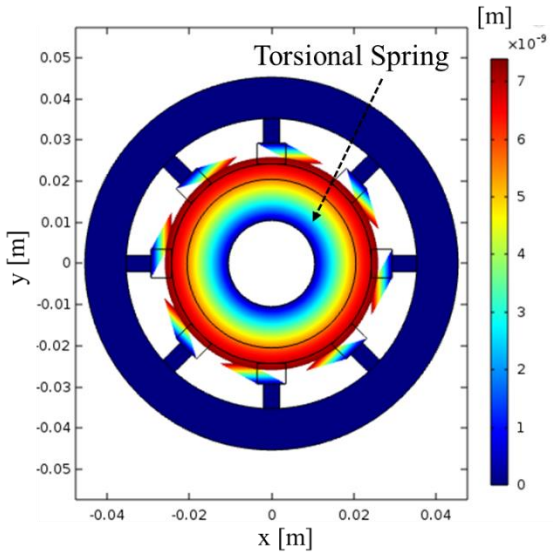

Figure 42. COMSOL result for transducer gripper validation.

Figure 42 shows static circumferential displacement amplitudes of the 2-D pipe model attached with a torsional spring. Displacements are generated by the transducer array, on which 20 V voltage is applied to its top and bottom surfaces. The transducer array is placed against the surface of the pipe by the transducer array gripper. The outer boundary of the gripper is fixed, so that its displacement is zero. 300 N inward radius direction force is applied to the outer surface of the gripper to mimic the force generated by a robot arm, which holds the transducer gripper in reality. The maximum displacement of 7.4×10^{-9} m is obtained at the outer boundary of the pipe as shown in Figure 42. With this statistic displacement as the excitation amplitude, a 3D finite element simulation is conducted for pipe of interest. The amplitude of a defect-reflected wave from a 120^{o} circumferential span, 3 mm axial span defect is 0.875 nm. For the transducers, the voltage associate with this displacement is 1.47 V. Therefore, the

defect-reflected wave is detectible with current transducer array system.

The 3-D drawing of the designed transducer gripper is generated in AutoCAD as shown in Figure 43. This transducer gripper has two parts, which have mirrored shapes with same dimensions except for the male and female joints. These two parts are connected by a pin, which is not included in the drawing.

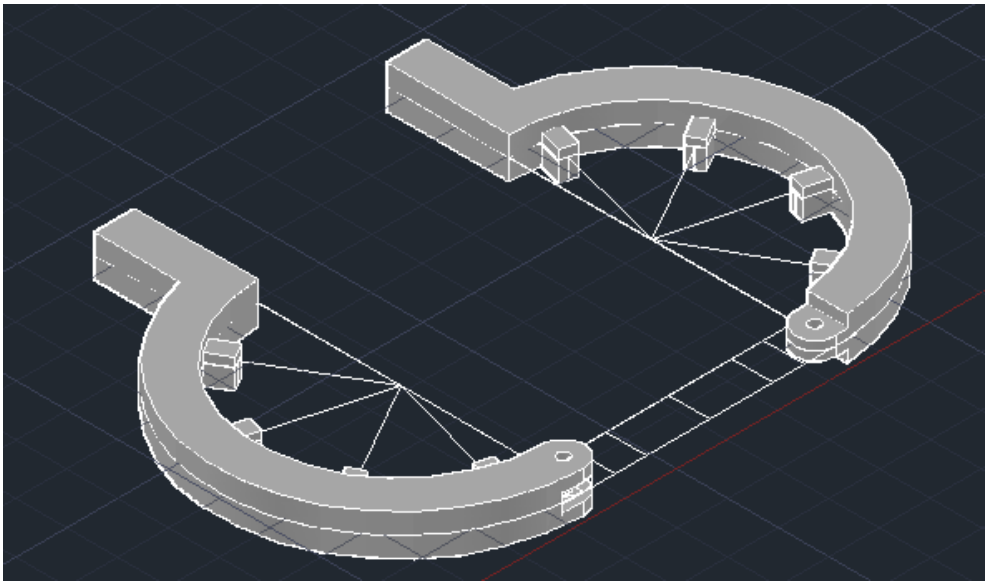

Figure 43. 3-D model of transducer gripper.

The designed 3-D gripper model was prototyped by a 3D printer (FOURTUS 400mc). The printing material is ABS-M30. The photo of the printed transducer gripper is shown in Figure 44.

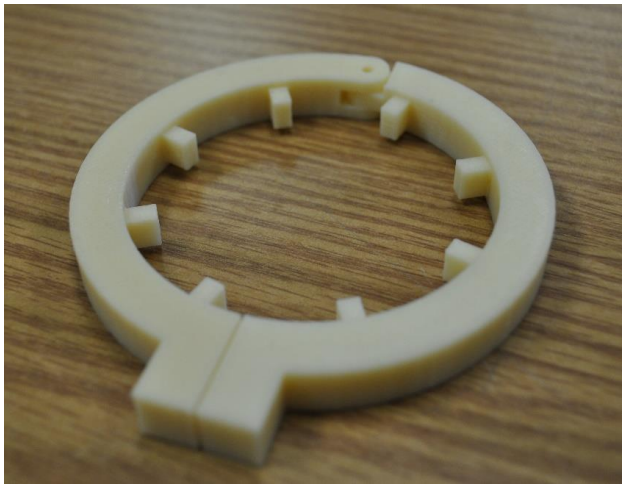

Figure 44. Photo of the 3D printed prototype of the transducer gripper.

5.2 Experimental Setup

As shown in the in-lab experimental setup of Figure 45, a National Instruments (NI) Data acquisition (DAQ) system is used to generate ultrasonic excitation and measure ultrasonic wave responses.

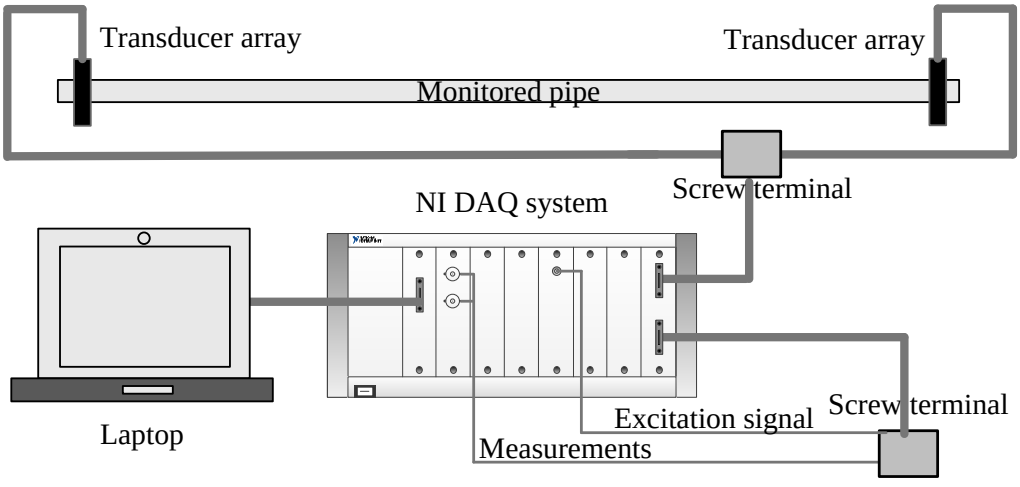

Figure 45. Experimental setup.

In particular, an ultrasonic excitation signal is generated from the Arbitrary Waveform Generator (NI PXI-542) and fed to each of the ultrasonic transducer arrays though the matrix switch (NI PXI-2536) simultaneously. The defect-reflected GUW measured by transducers is routed through a matrix switch and recorded in the digitizer module (NI PXIe-5122).

The experiment requires multiple excitations and data acquisition cycles to collect the measurement from all the transducers, because there are only two input channels in NI PXIe-5122. Each cycle is divided into two processes: the excitation process and the measurement process. During the excitation process, the matrix switch is set to connect NI Function Generator with transducers. The same excitation signal is sent to all excitation channels simultaneously. During the measurement process, the matrix switch is set to connect NI digitizer with transducers. The measurements are acquired from two out of all channels. The measurements from all the other channels can be obtained by repeating the same cycle multiple times.

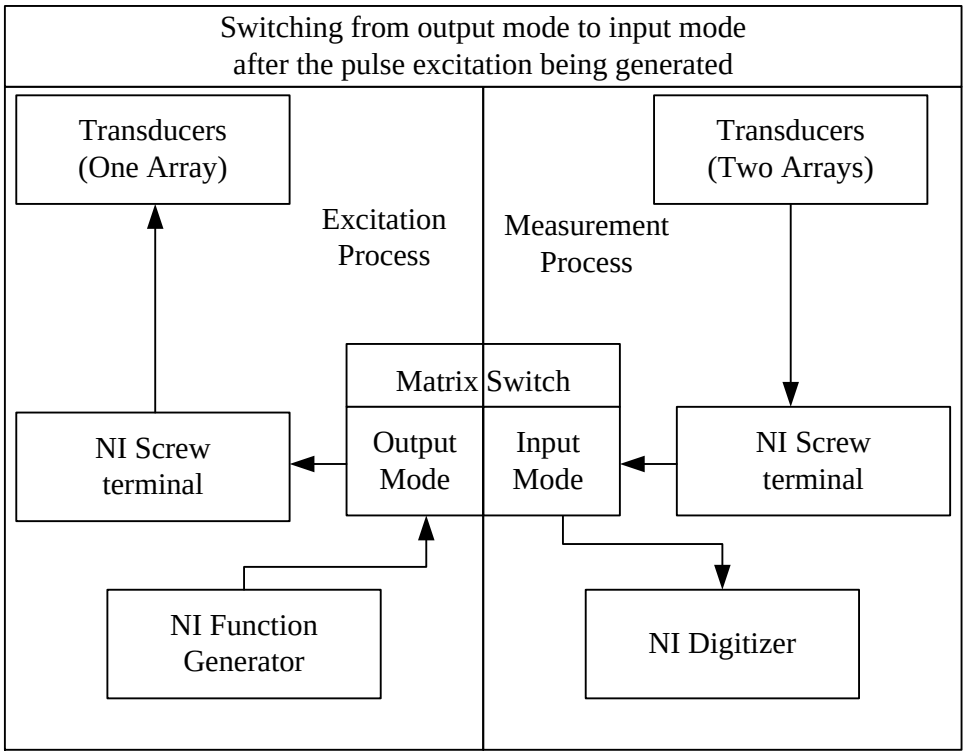

Figure 46. LabVIEW scripture design for the in-lab experiment.

The LabVIEW code for this experiment consists two parts the excitation process and the measurement process as well, as shown in Figure 46. In the excitation process, the aim of the LabVIEW script is to generate the desired the excitation by using a NI Function Generator. Once the function generator finished generating the signal, a trigger is sent to the matrix switch, and the whole system switches to the measurement process. In the measurement process, the Matrix switch to input mode and starts to read data from transducers from both the excitation transducer array and the measurement transducer array. Measurements are sent to the NI DAQ channels and saved to the Laptop.

Meanwhile, the matrix switch is set to output mode to send out the excitation to the power amplifier. There is a limitation of the maximum voltage that the NI function

generator can output. In case that more excitation power is needed, an ultrasonic power amplifier (ENI 200L Power Amplifier) is connected between the generator and the transducer array to drive transducers with a high power. A power amplifier can be deployed to increase the excitation voltage and in turn increase the SNR.

5.3 Conclusions

An experiment schema is presented in this section for experimental validation of the proposed SHM paradigms. The transducer made of APC 850 is chosen to generate the $T(0,1)$ GUW excitation. A transducer gripper is designed to place the transducer array mechanically. The design of the transducer gripper is validated by finite element simulation. The transducer gripper prototype is generated by 3-D printing. The experimental setup and procedure are also presented. The signal generation and the measurement acquisition are implemented by a NI DAQ system. The structure of the LabVIEW script for this experiment is presented.

6. SUMMARY

SHM with GUW over a small-diameter pipe is challenging, because defect-reflected GUW propagation characteristics are complicated. GUW propagation characteristics on a small-diameter pipe is analyzed by generating dispersion curves with both analytical and numerical methods. A proper frequency and a proper mode are chosen for the excitation based on the dispersion curves. It is also shown that dispersion curves are not sensitive to the diameter and the thickness changes for the small diameter.

Three SHM paradigms are presented for small-diameter pipe structures with GUW excitation.

In the first SHM paradigm, a creative design of the transducer array, dual transducer array, is presented. We demonstrate that a single array data acquisition system is not suitable for pipe structures when the MUSIC method is chosen as the data processing method. The defect location can only be detected when there is a transducer array at each end of the interested region. The simulations also show that, when the interested region of the pipe is bounded by dual ring-type transducer arrays, the axial location of the defect is correctly detected.

The uncertainty of the propagation path of the defect reflected GUW makes it is hard to detect the circumferential location of the defect. The second and the third paradigms are proposed to solve this issue.

With the same dual transducer array design, we proposed the second paradigm with a novel signal processing method, GD-MUSIC method. This paradigm can detect the circumferential location of the defect as well as the axial location of the defect. In

this method, the defect-reflected GUW is assumed to propagate along the geodesic path. This SHM paradigm is suitable for single defect cases.

The third paradigm is the based on the statistic method. The pipe is unwrapped with respect to different circumferential cuts. All different unrolled cases are referred as voters. The MUSIC signal processing method is applied to each different unwrapped case. The result from each unwrapped case is treated as a vote casted by each voter. The poll result gives the correct location of the defect in both circumferential direction and axial direction.

Finally, the experiment schema is proposed for future validation by experiments.

In the future work, the experiment will be conducted to validate all the three presented paradigm. Additionally, the signal processing method has the headroom for improvement on reducing the analyses error and detecting defects with even smaller defects.

REFERENCES

[1] C. R. Farrar, and K. Worden, "An introduction to structural health monitoring," *Philosophical Transactions of the Royal Society of London A: Mathematical, Physical and Engineering Sciences*, 2007, **365**, 303-315.

[2] S. W. Doebling, C. R. Farrar, M. B. Prime, and D. W. Shevitz, *Damage identification and health monitoring of structural and mechanical systems from changes in their vibration characteristics: a literature review (No. LA--13070-MS)*, Los Alamos National Lab, NM, 1996, 1-121.

[3] A. Raghavan, and C. E. S. Cesnik, "Review of guided-wave structural health monitoring," *Shock and Vibration Digest*, 2007, **39**, 91-116.

[4] P. Cawley, M. J. S. Lowe, D. N. Alleyne, B. Pavlakovic, and P. Wilcox, "Practical long range guided wave inspection-applications to pipes and rail," *Materials Evaluation*, 2003, **61**, 66-74.

[5] J. L. Rose, *Ultrasonic waves in solid media*, Cambridge university press, United Kingdom, 2004, 154-160.

[6] J. L. Rose, "A baseline and vision of ultrasonic guided wave inspection potential," *Journal of Pressure Vessel Technology Transactions of American Society of Mechanical Engineers*, 2002, **124**, 273-282.

[7] L-y. Sun, Xiao-d. Yang, and Yi-b. Li, "Research on transducer and frequency of ultrasonic guided waves in urban pipe inspection," *IEEE Conference on Industrial Electronics and Applications*, 2009, **4**, 2708-2711.

[8] T. Stepinski, "Structural Health Monitoring of Piping in Nuclear Power Plants," *Swedish Radiation Safety Authority*, 2011, **17**, 1-45.

[9] M. J. S. Lowe, D. N. Alleyne, and P. Cawley, "Defect detection in pipes using guided waves," *Ultrasonics*, 1998, **36**, 147-154.

[10] C. Ennaceur, P. Mudge, B. Bridge, M. Kayous, and T. H. Gan, "Application of the time reversal technique to the focusing of long-range ultrasound in pipelines," *Insight-Non-Destructive Testing and Condition Monitoring*, 2007, **49**, 217-223.

[11] H. Nishino, K. Ogura, T. Komatsu, and K, Yoshida, "Defect detection of a pipe using a guided wave generated by an efficient transduction with a reflector," *Japanese Journal of Applied Physics*, 2009, **48**, 1-7.

[12] T. Hayashi, K. Kawashima, Z. Sun, and J. L Rose, "Analysis of flexural mode focusing by a semi-analytical finite element method," *Journal of the Acoustical Society of America*, 2003, **113**, 1241-1248.

[13] Y. Jin, Y. Ying, and D. Zhao. "Data communications using guided elastic waves by time reversal pulse position modulation: Experimental study," *Sensors*, 2013, **13**, 8352-8376.

[14] D. Jacob, and P. Cawley, "The application of synthetic focusing for imaging crack-like defects in pipelines using guided waves," *IEEE Transactions on Ultrasonics, Ferroelectrics, and Frequency Control*, 2009, **56**, 759-771.

[15] R. Schmidt, "Multiple emitter location and signal parameter estimation," *IEEE Transactions on Antennas and Propagation*, 1986, **34**, 276-280.

[16] J. H. Han, and Y.-J. Kim, "Time–frequency beamforming for nondestructive evaluations of plate using ultrasonic Lamb wave," *Mechanical Systems and Signal Processing*, 2015, **54**, 336-356.

[17] J. Li, and J. L. Rose, "Angular-profile tuning of guided waves in hollow cylinders using a circumferential phased array," *IEEE transactions on ultrasonics, ferroelectrics, and frequency control*, 2002, **49**, 1720-1729.

[18] J. Li, and J. L. Rose, "Natural beam focusing of non-axisymmetric guided waves in large-diameter pipes," *Ultrasonics*, 2006, **44**, 35-45.

[19] K. Liu, Z. Wu, Y. Jiang, Y. Wang, K. Zhou, and Y. Chen, "Guided waves based diagnostic imaging of circumferential cracks in small-diameter pipe," *Ultrasonics*, 2016, **65**, 34-42.

[20] F. Deng, B. Wu, and C. He, "Time reversal method for guided wave inspection in pipes," *Frontiers of Mechanical Engineering in China*, 2008, **3**, 251-260.

[21] Z. Sun, L. Zhang, B. Gavigan, T. Hayashi, and J. L. Rose, "Ultrasonic flexural torsional guided wave pipe inspection potential," *American Society of Mechanical Engineers Pressure Vessels and Piping Conference*, 2003, **1**, 29-34.

[22] Z. Sun, J. L. Rose, W.J. Song, and T. Hayashi, "Non-axisymmetric wave focusing in pipe inspection," *AIP Conference Proceedings*, 2003, **22**, 244-249.

[23] J. Mu, L. Zhang, and J. L. Rose. "Defect circumferential sizing by using long range ultrasonic guided wave focusing techniques in pipe," *Nondestructive Testing and Evaluation*, 2007, **22**, 239-253.

[24] J. Li, “On circumferential disposition of pipe defects by long-range ultrasonic guided waves,” *Journal of pressure vessel technology*, 2005, **127**, 530-537.

[25] Z. Liu, Q. Xu, Y. Gong, C. He, and B. Wu, “A new multichannel time reversal focusing method for circumferential Lamb waves and its applications for defect detection in thick-walled pipe with large-diameter,” *Ultrasonics*, 2014, **54**, 1967-1976.

[26] B. Zaghari, V. Humphrey, and M. Moshrefi-Torbati, “Dispersion behavior of torsional guided waves in a small diameter steel gas pipe,” *19th International Conference on Automation and Computing (ICAC)*, 2013, **19**, 1-6.

[27] H. Lamb, “On waves in an elastic plate,” *Proceedings of the Royal Society of London A: Mathematical, Physical and Engineering Sciences*, 1917, **93**. 114–128.

[28] C. Aristegui, M. J. S. Lowe, and P. Cawley, “Guided waves in fluid-filled pipes surrounded by different fluids,” *Ultrasonics*, 2001, **39**, 367-375.

[29] Mini Tools from Teletest Focus Plus, http://www.teletestfocus.com/teletest-focus-plus/mini-tools/.

[30] J. H. Han, Y.-J. Kim, and M. Karkoub, “Wave propagation modeling of fluid-filled pipes using hybrid analytical/two-dimensional finite element method,” *Wave Motion*, 2014, **51**, 1193-1208.

[31] J. H. Han, and Y.-J. Kim, “Ultrasonic Lamb wave propagation characteristics in hollow cylindrical pipes,” *Proceedings of Inter-Noise*, 2012, **8**, 1-12.

[32] P. Smith, *The fundamentals of piping design*, Gulf Publishing Company, TX, 2013, 62

[33] D. N. Alleyne, M. J. S. Lowe, and P. Cawley, "The reflection of guided waves from circumferential notches in pipes," *Journal of Applied mechanics*, 1998, **65**, 635-641.

[34] D. N. Alleyne, T. Vogt, and P. Cawley, "The choice of torsional or longitudinal excitation in guided wave pipe inspection," *Insight-Non-Destructive Testing and Condition Monitoring*, 2009, **51**, 373-377.

[35] J. N. Reddy, *Introduction to the Finite Element Method*, McGraw Hill, NY, 1993.

[36] A. V. Oppenheim, R. W. Schafer, and J. R. Buck. *Discrete-Time Signal Processing*, Prentice Hall, NJ, 1999, 262-468.

[37] S. Jiang, K. Mansour, and, Y.-J. Kim, "High-Resolution Ultrasonic NDE Imaging Method with Virtually Expanded Circumferential Aperture in Small-Diameter Cylindrical Oil/Gas Pipes," *INTER-NOISE and NOISE-CON Congress and Conference Proceedings*, 2016, **252**, 174-183.

[38] A. Belouchrani, and M. G. Amin, "Time-frequency MUSIC," *IEEE Signal Processing Letters*, 1999, **6**, 109-110.

[39] J. Achenbach, *Wave propagation in elastic solids*, Elsevier, New York, 2012, 326-356.

[40] ANSYS 17.0, http://www.ansys.com/products/structures/vibrations.

[41] W. Soedel, *Vibrations of shells and plates*, CRC Press, NY, 2004.

[42] Z. Liu, C. He, B. Wu, X. Wang, and S. Yang, "Circumferential and longitudinal defect detection using T (0, 1) mode excited by thickness shear mode piezoelectric elements," *Ultrasonics*, 2006, **44**, 1135-1138.

[43] W. Wang, J. P. Lynch, and H. LI, “Damage Detection in Metallic Plates using d36 Piezoelectric Phased Arrays,” *European Workshop On Structural Health Monitoring*, 2016, **8**, 1-10.

[44] O. Bareille, M. Kharrat, W. Zhou, and M. N. Ichchou, “Distributed piezoelectric guided-T-wave generator, design and analysis,” *Mechatronics*, 2012, **22**, 544-551.

[45] COMSOL Multiplysicas Modeling Software, http:// www.comsol.com.

APPENDIX A

ANSYS APDL SCRIPT FOR ANSI 4 INCH SCHEDULE 5 CASE

```
Finish
/CLE
/FILNAM,pipe, 0         ! Jobname
/TITLE, pipe
/PREP7               ! Enter PREP7
!!!!!!!!!!!!!!!!!!!!!!!!!!!!!!!!!!!!
!! define parameters (m)
!!!!!!!!!!!!!!!!!!!!!!!!!!!!!!!!!!!!
! schedule 5
! 4 inch OD
pipe_RO = 114.3e-3/2 !meter
pipe_d = 2.1082e-3 !meter
pipe_RI = pipe_RO-pipe_d
pipe_L = 1
mnt_s = 0
mnt_e = 0
defect_z = 0.4
defect_w = 6E-3
ANGLE = 60  !deg
d_pipe_L = 2*6e-3
ANGLE_diff = 90
!!!!!!!!!!!!!!!!!!!!
!! TIME TABLE
!!!!!!!!!!!!!!!!!!!!
table_L = 815
TM_INCR = 1/1e6
TM_START = TM_INCR
TM_END =  table_L*TM_INCR
!!!!!!!!!!!!!!!!!!!!!!!!!!!!!!!!!!!!!!!!
!! GEOMETRY
!!!!!!!!!!!!!!!!!!!!!!!!!!!!!!!!!!!!!!!!
CYL4,0,0,pipe_RO        !1
CYL4,0,0,pipe_RI         !2
ASBA,1,2                 !ringe
VEXT, ALL, , , , , pipe_L               ! extrude
WPOFFS, 0, 0, defect_z                      ! defect surface
PCIRC,  1e-3,  25E-2,  (180-ANGLE)/2-ANGLE_diff,  180-(180-ANGLE)/2-
ANGLE_diff
VOFFST, 11, defect_w, 0     !
VSBV, 1, 2   ! boolean remove defect volum
!!!!!!!!!!!!!!!!!!!!!!!!!!!!!!!!!!!!!!!!!!!!!!!!!!!!!!!!!!!!!!!!!!!!
!! material
!!!!!!!!!!!!!!!!!!!!!!!!!!!!!!!!!!!!!!!!!!!!!!!!!!!!!!!!!!!!!!!!!!!
MP,EX,1,1.93E11                  ! Young's modulus
MP,PRXY,1,0.29           ! Poisson's ratio
MP,DENS,1,7889           ! Density
DMPSTR, 0.01
```

```
!!!!!!!!!!!!!!!!!!!!!!!!!!!!!!!!!!!!!!!!!!!!
! step 1: divide volum by workplane
!!!!!!!!!!!!!!!!!!!!!!!!!!!!!!!!!!!!!!!!!!!!
VSBW,ALL
KWPLAN, ,32,31,29
VSBW,ALL
KWPLAN, ,27,28,25
VSBW,ALL
KWPLAN, ,27,28,35
VSBW,ALL
LSEL, S, LOC, Z, 0
LSEL, U, LINE,,13
LSEL, U, LINE,,67
LSEL, U, LINE,,68
LSEL, U, LINE,,94
LSEL, A, LOC, Z, pipe_L
LSEL, U, LINE,,99
LSEL, U, LINE,,80
LSEL, U, LINE,,83
LSEL, U, LINE,,108
LSEL, A, LOC, Z, defect_z
LSEL, U, LINE,,41
LSEL, U, LINE,,69
LSEL, U, LINE,,15
LSEL, U, LINE,,37
LSEL, A, LOC, Z, defect_z+defect_w
LSEL, U, LINE,,14
LSEL, U, LINE,,42
LSEL, U, LINE,,114
LSEL, U, LINE,,38
LESIZE,ALL,,3,,,1  ! 1 degree
!!!!!!!!!!!!!!! thickness
! z  = 0
LSEL, S, LINE,,94
LSEL, A,LINE,,13
LSEL, A, LINE,,67
LSEL, A, LINE,,68
! z = pipe_L
LSEL, A, LINE,,99
LSEL, A, LINE,,80
LSEL, A, LINE,,83
LSEL, A, LINE,,108
! z = defect_z
LSEL, A, LINE,,41
LSEL, A, LINE,,69
LSEL, A, LINE,,15
LSEL, A, LINE,,37
! z = defect_z+defect_w
LSEL, A, LINE,,14
LSEL, A, LINE,,42
LSEL, A, LINE,,114
LSEL, A, LINE,,38
LESIZE,ALL,,,2,,1 ! Adjust line divisions based on DESIZE,
force adjustments
```

```
     !!!!!!!!!!!!!!!! straight lines
     LSEL,NONE
     LSEL,ALL
     LSEL,U,LOC,z,0
     LSEL,U,LOC,z,pipe_L
     LSEL,U,LOC,z,defect_z
     LSEL,U,LOC,z,defect_z+defect_w
     LESIZE,ALL,6e-3,,,, ! Adjust line divisions based on DESIZE, force
adjustments
     !!!!!!!!!!!!!!!!!!!!!!!!!!!!!!!!!!!!!!!!!!!!
     !! mesh
     !!!!!!!!!!!!!!!!!!!!!!!!!!!!!!!!!!!!!!!!!!!!
     ET,1,solid95   ! 2D brick 20-node 8+8+4
     MSHAPE,0,3D
     MSHKEY,1 ! Use mapped meshing if possible
     VSWEEP, all
     /ESHAPE,1
     !LPLOT
     !/PNUM,LINE,1
     !FINISH
     !!!!!!!!!!!!!!!!!!!!!!!!!!!!!!!!!!!!!!!!!!!!!!!!!!!!!!!!!!!!!!!!!!!!!!!
     !!! select nodes
     !!!!!!!!!!!!!!!!!!!!!!!!!!!!!!!!!!!!!!!!!!!!!!!!!!!!!!!!!!!!!!!!!!!!!!!
     csys,1
     nrotat,all
     ! circle
     mnt_angle = 6
     *DO,ID_N,1,60,1
        node%ID_N% = node( pipe_RO, mnt_angle*(ID_N-1),0) ! z = 0
        node10%ID_N% = node( pipe_RO, mnt_angle*(ID_N-1),pipe_L)
     *ENDDO
     ! circle
     *DO,ID_2d,1,20,1
        node20%ID_2d% = node( pipe_RO, 90,d_pipe_L*ID_2d) ! z = 0
        node30%ID_2d% = node( pipe_RO, 90,pipe_L-d_pipe_L*ID_2d)
     *ENDDO
     FINISH
     !!!!!!!!!!!!!!!!!!!!!!!!!!!!!!
     !!!   tran analysis
     !!!!!!!!!!!!!!!!!!!!!!!!!!!!!!
     !  Apply Loads and Obtain the Solution
     /SOLU                       ! Enter SOLUTION
     ANTYPE,TRANS                ! Transient analysis
     TRNOPT,FULL                 ! Full method
     !!!!!!!!!!!!!!!!!!!!!!
     !! APPLY LOAD  !!!!!!!!
     !!!!!!!!!!!!!!!!!!!!!!
     NSEL,S,NODE, ,node1  !
     *DO,ID_f,1,60,1
       NSEL,A,NODE, ,node%ID_f%
     *ENDDO
     *DIM,force,table,table_L,1,1,TIME
     *TREAD,force,force_load815,txt
     !! force
```

```
F,all,FY,%force%,,,
OUTRES,ALL,LAST,
ALLSEL
*DO,TM,TM_START,TM_END,TM_INCR
KBC,0                    ! Ramped or stepped loads 0 ramped
TIME,TM
AUTOTS,ON                  ! Auto time stepping
DELTIM, TM_INCR/5 , TM_INCR/5, TM_INCR/2, ON
SOLVE
*ENDDO
ALLSEL
FINISH
!!!!!!!!!!!!!!!!!!!!!!!!!!!!!!!!!!!!!!!!!!!!!!!!
!!!!!!!!!  output
!!!!!!!!!!!!!!!!!!!!!!!!!!!!!!!!!!!!!!!!!!!!!!!!
/POST1
NSEL,S,NODE, ,node1
*DO,ID_MNT,1,60,1
NSEL,A,NODE, ,node%ID_MNT%
NSEL,A,NODE, ,node10%ID_MNT%
*ENDDO
*DO,ID_MNT_2D,1,20,1
NSEL,A,NODE, ,node20%ID_MNT_2D%
NSEL,A,NODE, ,node30%ID_MNT_2D%
*ENDDO
*GET,N_SIZE,NODE,,COUNT !!Number of nodes in the selected set
*GET,S_SIZE,ACTIVE,0,SET,NSET!!Getting the number of sets
*DIM,ACC_ARRAY,ARRAY,S_SIZE,(N_SIZE+1) Creating Array as per
number of sets as rows
!! save locations
n=0
*CFOPEN,loc,txt  !
*DO,j,1,N_SIZE,1!!Do Loop for storing the values to the Array
n=NDNEXT(n)
*VWRITE,j
(F8.0,$)
*VWRITE,n
(F8.0,$)
loc_nx = NX(n)
*VWRITE,loc_nx
(ES20.6E6,$)
loc_ny = NY(n)
*VWRITE,loc_ny
(ES20.6E6,$)
loc_nz = NZ(n)
*VWRITE,loc_nz
(ES20.6E6,)
*ENDDO
*CFCLOSE
FINISH
/POST26
NUMVAR,200
!FILE,pipe,rst
n=0
```

```
*CFOPEN,acc_y,txt
*VWRITE,
('      Time  ',$)
*DO,j,2,(N_SIZE+1),1
n=NDNEXT(n)
NSOL,j,n,ACC,Y, AY_%j%,
VGET,ACC_ARRAY(1,1),1
VGET,ACC_ARRAY(1,j),j
*IF,j,LT,(N_SIZE+1),THEN
*VWRITE,n
(F8.0,$)
*ENDIF
*IF,j,EQ,(N_SIZE+1),THEN
*VWRITE,n
(F8.0)
*ENDIF
*ENDDO
*DO,i,1,S_SIZE,1
*DO,j,1,(N_SIZE+1),1
a=ACC_ARRAY(i,j)
*IF,j,LT,(N_SIZE+1),THEN
*VWRITE,a
(ES20.6E6,$)
*ENDIF
*IF,j,EQ,(N_SIZE+1),THEN
*VWRITE,a
(ES20.6E6)
*ENDIF
*ENDDO
*ENDDO
*CFCLOSE
```